iScience

CellPress
OPEN ACCESS

Article

Antithrombogenic polysaccharide coatings to improve hemocompatibility, protein-repellence, and endothelial cell response

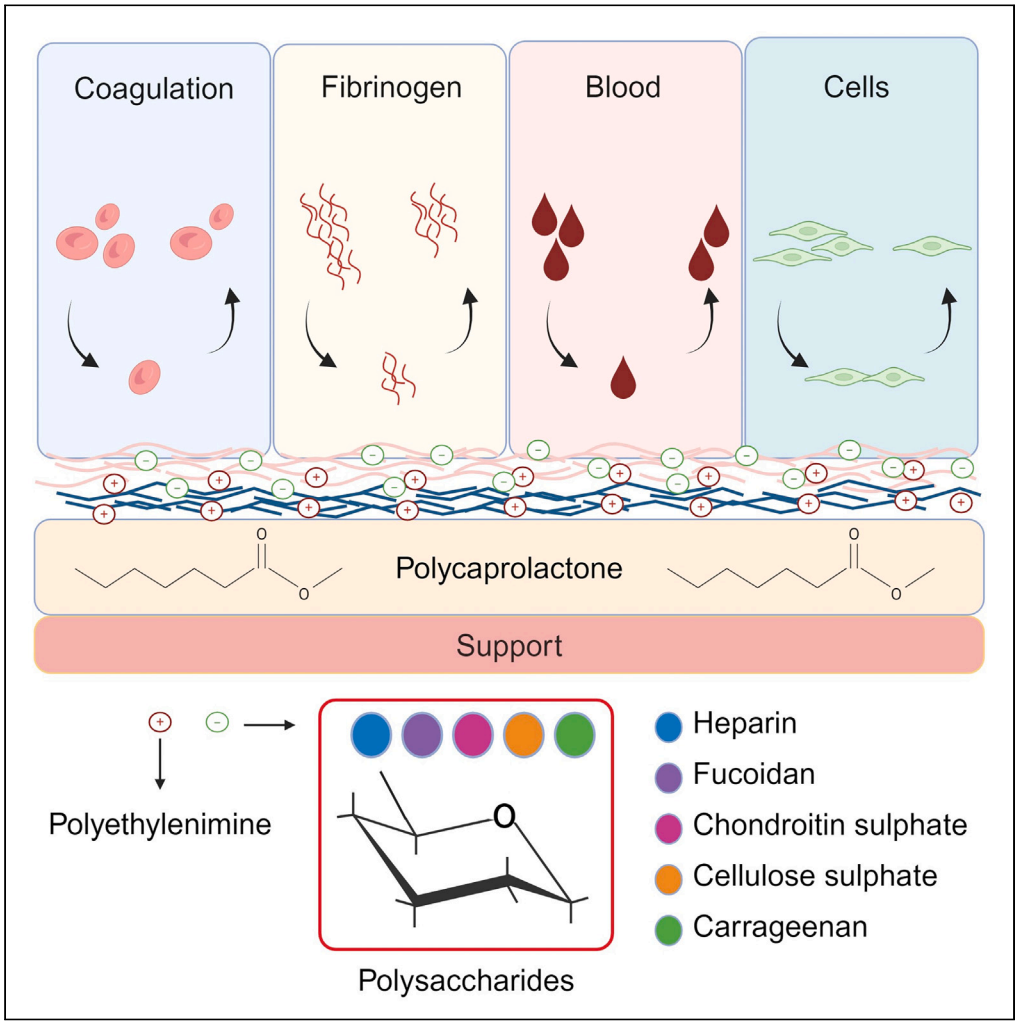

Matej Bračič, Bence M. Nagy, Olivija Plohl, ..., Karin Stana Kleinschek, Chandran Nagaraj, Tamilselvan Mohan

n.chandran@medunigraz.at (C.N.)
tamilselvan.mohan@tugraz.at (T.M.)

Highlights

Functionalization of vascular materials with sulfated polysaccharides (SPS)

Enhanced hemocompatibility, protein-repellence, reduced blood adhesion

The SPS coatings promoted endothelial cells adhesion and biocompatible

The coatings represent a modern approach to design vascular grafts and stents

Bračič et al., iScience 27, 110692
September 20, 2024
https://doi.org/10.1016/j.isci.2024.110692

iScience

CellPress
OPEN ACCESS

Article

Antithrombogenic polysaccharide coatings to improve hemocompatibility, protein-repellence, and endothelial cell response

Matej Bračič,[1,8] Bence M. Nagy,[2] Olivija Plohl,[1,8] Florian Lackner,[3,8] Tobias Steindorfer,[3,8] Roland C. Fischer,[4] Thomas Heinze,[5] Andrea Olschewski,[2,6] Karin Stana Kleinschek,[3,7,8] Chandran Nagaraj,[2,*] and Tamilselvan Mohan[1,3,8,9,*]

SUMMARY

Polyester biomaterials play a crucial in vascular surgery, but suffer from unspecific protein adsorption, thrombogenicity, and inadequate endothelial cell response, which limit their success. To address these issues, we investigated the functionalization of polyester biomaterials with antithrombogenic polysaccharide coatings. A two-step and water-based method was used to coat cationized polycaprolactone with different sulfated polysaccharides (SPS), which resulted in long-term stability, tunable morphology, roughness, film thickness, chemical compositions, zeta potential, and water content. The coatings significantly increased the anticoagulant activity and reduced the thrombogenicity of polycaprolactone, particularly with highly sulfated heparin and cellulose sulfate. Less SPS, such as chondroitin sulfate, fucoidan, and carrageenan, despite showing reduced anticoagulant activity, also exhibited lower fibrinogen adsorption. The adhesion and viability of human primary endothelial cells cultured on modified polycaprolactone correlated with the type and sulfate content of the coatings.

INTRODUCTION

Biomaterials play a crucial role in the development of vascular grafts or blood contacting devices that are inserted into or onto the surface of the body to replace a missing biological structure or support a damaged one.[1,2] Key aspects of biomaterials for vascular grafts include biocompatibility, physicochemical, and structural properties, integration with cells (e.g., endothelial cells, ECs) or tissues, functionalities, prevention of thrombosis formation, etc.[3,4] Materials such as metals, polymers, proteins, composites, and natural (autologous) tissue2s have been used and the introduction of new bioactive functional groups on the surfaces of vascular grafts is an ongoing progress.[2,4] Natural polymers or tissues (e.g., collagen, fibroin, and decellularized tissue) show good compatibility with vascular tissue, but usually suffer from mechanical instability and batch-dependent differences in physicochemical properties.[5] Synthetic polymers (e.g., polyethylene terephthalate [PET], polytetrafluoroethylene [PTFE] or polyurethane [PU]), on the other hand, offer good mechanical stability as well as high reproducibility and processability, but are not biodegradable, have no functional groups and can cause thrombotic occlusions.[5,6] This limits the use of these polymers in small-diameter vascular grafts (SDVGs, <6 mm).[7] In contrast, biodegradable polyesters such as polycaprolactone (P) are often used for the production of SDVGs as they have the required mechanical and biocompatible properties and are cost-effective.[8,9] P has been approved by the Food and Drug Administration for various biomedical applications such as resorbable sutures, scaffolds for tissue engineering, and drug delivery systems.[10] Nevertheless, P lacks molecular motifs for biological recognition, leading to uncontrolled adsorption of blood proteins and subsequent thrombosis, which in turn prevents endothelialization. Therefore, various surface modifications with bioactive molecules such as gelatin, collagen, peptides, phosphorylcholine-based polymers, silicon, or chitosan have been performed to improve the adhesion, spreading, and proliferation of ECs.[10] Until now, various approaches have been developed to alter the surface properties of P. These include blending or co-electrospinning, surface graft polymerization, plasma-treatments, wet chemical modification (i.e., surface hydrolysis), etc.[10,11] All these surface modification approaches often require multiple/tedious or expensive coating steps, stability,[12] leading to the destruction of

[1]University of Maribor, Faculty of Mechanical Engineering, Laboratory for Characterisation and Processing of Polymers, Smetanova ulica17, 2000 Maribor, Slovenia
[2]Ludwig Boltzmann Institute for Lung Vascular Research, Stiftingtalstrasse 24, 8010 Graz, Austria
[3]Graz University of Technology, Institute for Inorganic Chemistry, Stremayrgasse 9, 8010 Graz, Austria
[4]Graz University of Technology, Institute of Chemistry and Technology of Biobased System, Stremayrgasse 9, 8010 Graz, Austria
[5]Center of Excellence for Polysaccharide Research, Institute of Organic Chemistry and Macromolecular Chemistry, Friedrich Schiller University of Jena, Humboldtstraße 10, 07743 Jena, Germany
[6]Department of Anaesthesiology and Intensive Care Medicine, Medical University of Graz, 8036 Graz, Austria
[7]University of Maribor, Institute of Automation, Faculty of Electrical Engineering and Computer Science, Koroška cesta 46, 2000 Maribor, Slovenia
[8]Members of the European Polysaccharide Network of Excellence (EPNOE)
[9]Lead contact
*Correspondence: n.chandran@medunigraz.at (C.N.), tamilselvan.mohan@tugraz.at (T.M.)
https://doi.org/10.1016/j.isci.2024.110692

the structural integrity of P. In this context, simple methods, especially water-based coating techniques and use of natural polysaccharides (PS), which show good hemo-/biocompatibility, and functional properties are in high demand.[13–15]

In this paper, emphasis is laid on antithrombogenic properties of various sulfated and water-soluble PS as functional (bio)coatings for P-thin films and their effects on adhesion and growth of ECs. The development of functional (bio)coatings that prevent unspecific protein adsorption and blood clotting and support EC adhesion and growth is crucial for the preparation of SDVG.[10,16,17] Sulfated polysaccharides (SPS) are known to be an excellent anticoagulant.[14,18,19] Heparin (Hep), which is considered as the gold standard among antithrombogenic drugs, is used to coat biomaterials that come into contact with blood to prevent thrombosis.[20] However, despite its ability to prevent thrombus formation, heparin interacts with platelets and macrophages and can cause the formation of neointima or hemorrhage, creating an unfavorable environment for the adhesion and growth of EC on the surface of biomaterials.[21,22] Furthermore, heparin is expensive, and it is reasonable for researchers to look at other inexpensive synthetic and plant-based alternative polymers that have antithrombogenic properties and provide favorable conditions for EC growth. These alternatives include SPS such as fucoidan (Fu),[13] chondroitin sulfate (CS),[23] carrageenan (Carr), or cellulose sulfate (CellS).[14] For example, CS coatings have already been shown to promote adhesion and survival of EC and reduce unspecific protein adsorption on solid supports.[23] Fu has been extensively studied for its anticoagulant effect, showing great potential, but studies on its antithrombogenic effect as a coating on solid surfaces are scarce. Recently, Ozaltyn et al. showed that Fu coated on plasma cationized PET imparted anticoagulant properties to the PET surface, as determined by prothrombin time, activated partial thromboplastin time and thrombin time.[13] Similarly, CellS coated on PET showed antithrombogenic activity by reducing the clot formation time.[14] Researchers have also utilized several synthetic materials as antithrombogenic coating materials, including polyethylene glycol, phosphorylcholine, poly(2-methacryloyloxyethyl phosphorylcholine), poly(lactic-co-glycolic acid), rivaroxaban, apixaban, and silicone.[12,24] While these antithrombogenic materials effectively reduce clot formation, they also exhibit several disadvantages, such as residual thrombogenicity, immune response, lack of bioactivity, stability issues, and biocompatibility challenges.[25] In contrast, the SPS offer several advantages, including anticoagulant and anti-inflammatory activity, biocompatibility, hydrophilicity, versatility, and natural origin.[26,27] These properties make SPS highly desirable and often superior for antithrombogenic applications compared to many other synthetic alternatives.

However, comprehensive studies comparing the antithrombogenicity of different SPS as coatings on thin solid P surfaces and their effects on EC adhesion and growth are scarce. In contrast to the work that has reported vascular grafts based on P nanofibres or membranes, in this work we investigated the functionalization of P-thin films with different SPS including Hep, Fu, CellS, Carr, and CS which have different physicochemical properties and degrees of sulfation. The functionalization was performed by decorating the P surfaces first with cationic polyethyleneimine (PE) and then with negatively charged SPS in a non-destructive and water-based two-step process. In this way, P surfaces can be tailored with varying degrees of wettability, morphology, charges, chemical composition, and hydration forces without the need for harsh physical or chemical treatment. The influences of these physicochemical properties of SPS coated surfaces on protein adsorption, anticoagulant activity, and EC interactions have not yet been reported and are of critical importance for the preparation of vascular grafts. Furthermore, the changes in ECs shape, conformation, and metabolic activity upon interaction with different SPS coated P surfaces are largely unknown. Many of these relevant parameters that determine the final properties of the materials, can only be studied with great effort on P thin solid films. Therefore, the investigation of P thin films as model substrates for SDVG with defined surface and morphology could be a possible solution to this problem. Especially for the use of such materials in biomedical applications, the knowledge of the exact nature, morphology, adsorption/crosslinking behavior as well as biocompatibility and processing properties is of particular importance. Basic studies of the adsorption of SPS or the interactions of proteins with thin solid surfaces/films can be carried out using techniques such as quartz crystal microbalance with dissipation (QCM-D), which can be used to measure the deposition of mass and the viscoelastic properties of the adsorbed layer.[28–30] QCM was used to evaluate the clotting time, fibrin formation rate and deposition, and viscoelastic properties of the formed blood clot on the SPS coated layers. Such studies focusing on the formation of blood clot with QCM-D are rare despite their potential.

In this study, following the charge analysis of SPS (Hep, CS, Carr, Fu, and CS) in solution, the activated partial thrombin time (APTT) was used as a standard test to evaluate the influence of all PS solutions on human blood plasma coagulation times. Subsequently, we investigated the functionalization of P thin films with SPS. Functionalization was performed by *in-situ* QCM-D adsorption or dip-coating. The SPS coated surfaces were characterized in terms of their morphology, wettability, thickness, charges, and chemical composition. QCM-D was used to determine the adsorption behavior of fibrinogen. The same instrument was used to determine the anticoagulant properties of the coated surfaces. These properties were correlated with the adhesion and growth of primary human pulmonary artery endothelial cells (hECs) on the materials. Understanding the interaction of unspecific protein interactions, human blood plasma and ECs with the SPS coated P materials described here should pave the way for the development of implantable, degradable SDVGs.

RESULTS AND DISCUSSION

Activated partial thromboplastin time

Figure 1A shows the concentration-dependent APTT of SPS in solution. It can be seen that the APTT for each polysaccharide is concentration dependent and it increased with increasing polysaccharide concentration. This is more pronounced for Hep and CellS compared to all other SPS (see Table 1). The anticoagulant effect of a polysaccharide can be compared with other PS by comparing the slopes of the linear trends of their APTT versus concentration data and the absolute APTT values at a given concentration. The reference (PBS buffer, dotted red line) has a slope of zero because all APTT data of the PS were normalized to the reference. A steeper slope (up to 10 times) was observed for CellS and

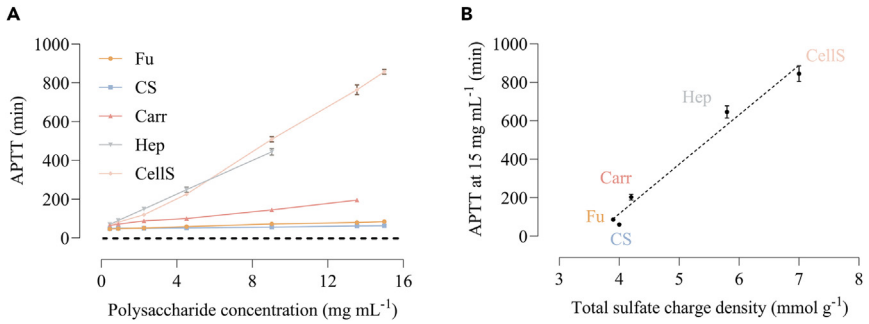

Figure 1. Activated partial thrombin time (APTT) of sulfated polysaccharides

(A) APTT vs. polysaccharide concentration (n = 3) and (B) APTT vs. total charge density at a polysaccharide concentration of 15 mg mL^{-1} (n = 3), and values are presented as ± SD.

Hep, indicating their superior anticoagulant effect at increasing concentrations. Interestingly, CellS (55.8 min/mg mL^{-1}) shows a steeper slope than Hep (40.4 min/mg mL^{-1}) and also a higher absolute APTT value (854.9 min vs. 657.0 min) at its maximum concentration (15 mg mL^{-1}). At lower concentrations (>5 mg mL^{-1}), no major differences in the APTT value were observed for all samples. The APTT value of all samples at the highest concentration (15 mg mL^{-1}) as a function of sulfate content is shown in Figure 1B. As expected, Hep ($DS_{sulfate}$: 2.4, sulfate content: 5.8 mmol g^{-1}) showed higher anticoagulant activity compared to the other anticoagulants (except CellS). Interestingly, CellS ($DS_{sulfate}$: 2.6, sulfate content: 7 ± 0.1 mmol g^{-1}) outperformed the anticoagulant activity not only of the gold standard Hep, but also of other SPS. This may be due to a higher DS or sulfate content of CellS (see Table 1). The APTT value determined in this work is several-fold higher than the value reported for CellS with the $DS_{sulfate}$ of 1.66.[14] After CellS, the maximum APTT value was obtained for Carr, followed by Fu and CS. These results show that the anticoagulant activity or APTT value is strongly dependent on the sulfate content of the PS. This is consistent with APTT test results published by other authors.[29,31] Overall, the SPS polysaccharide performance in the APTT is as follows: CS < Fu < Carr < Hep < CellS. In some cases, a deviation from the linear trend can be observed, as the anticoagulant activity depends on many other factors besides charge density and DS, such as the chemical structure of the polysaccharide backbone (see Table S1), molecular weight, and position of the sulfate groups.[32]

Surface functionalization of polycaprolactone thin films with sulfated polysaccharides

Surface functionalization of P thin films was performed *in-situ* by adsorption of various SPS differing in their charge (sulfate and carboxyl content), structure and function. Since the direct adsorption of negatively charged SPS on the neat P surfaces was not possible, we first functionalized the P surfaces with cationically charged multi-branched PE via irreversible adsorption.[33–35] Afterward, the PE surfaces were adsorbed with SPS through an electrostatic interaction (see Figure 2). The adsorption of PE on the P surfaces was done with QCM-D (see Figure S1), which showed that the PE adsorbed irreversibly on P. It is suggested that a strong affinity of PE for P surfaces is due to electrostatic interactions and hydrogen bonding.[34,35] Figures 3A–3C show the changes in QCM-D frequency (Δf_3) and dissipation (ΔD_3) and deposited mass (mg m^{-2}) for the adsorption of SPS on PE decorated P surfaces. A strong decrease in Δf_3 and an increase in ΔD_3 were observed during the adsorption of SPS. Over 90% of the adsorption occurred in the first couple of minutes due to a strong electrostatic interaction between the cationic PE and the anionic SPS.[19,33,36,37] After rinsing with NaCl and water, the Δf_3 was partly reversed, an indication that the loosely bound materials were removed from the surface. Interestingly, the less charged CS (Δf_3: −51.6Hz ± 1.8, 8.9 ± 0.3 mg m^{-2}) and Fu (Δf_3: −50.8Hz ± 2.2, 8.6 ± 0.5 mg m^{-2}) coated surfaces showed maximum adsorption after rinsing with water. On the other hand, the highly charged Hep and CellS showed the lowest adsorption with Δf_3 of 11.2 ± 2.2 (1.9 ± 0.1 mg m^{-2}) and 15.3 ± 2.5 (2.9 ± 0.3 mg m^{-2}), respectively. It can be assumed that the reduced charges and the associated lower solubility of CS and Fu were responsible for the maximum adsorption.[38–40] Other factors such

Table 1. List of sulfated polysaccharides (SPS) used for functionalization of P films

	Number of charges determined by titration (mmol g^{-1})			
Sulfated Polysaccharides	Sulfate	Carboxyl	Total	Molecular weight (kDa)
6-Chondroitin sulfate (CS)	3.0 ± 0.0	1.3 ± 0.0	4.3 ± 0.0	20–30
Fucoidan (Fu)	3.9 ± 0.1	*	3.9 ± 0.1	20–200
ι-Carrageenan (Carr)	4.2 ± 0.0	*	4.2 ± 0.0	20–30
Heparin (Hep)	4.4 ± 0.1	1.4 ± 0.1	5.8 ± 0.1	16–19
Cellulose sulfate (CellS)	7.0 ± 0.3	*	7.0 ± 0.3	672

*No carboxyl groups present in the chemical structure of the polymer.

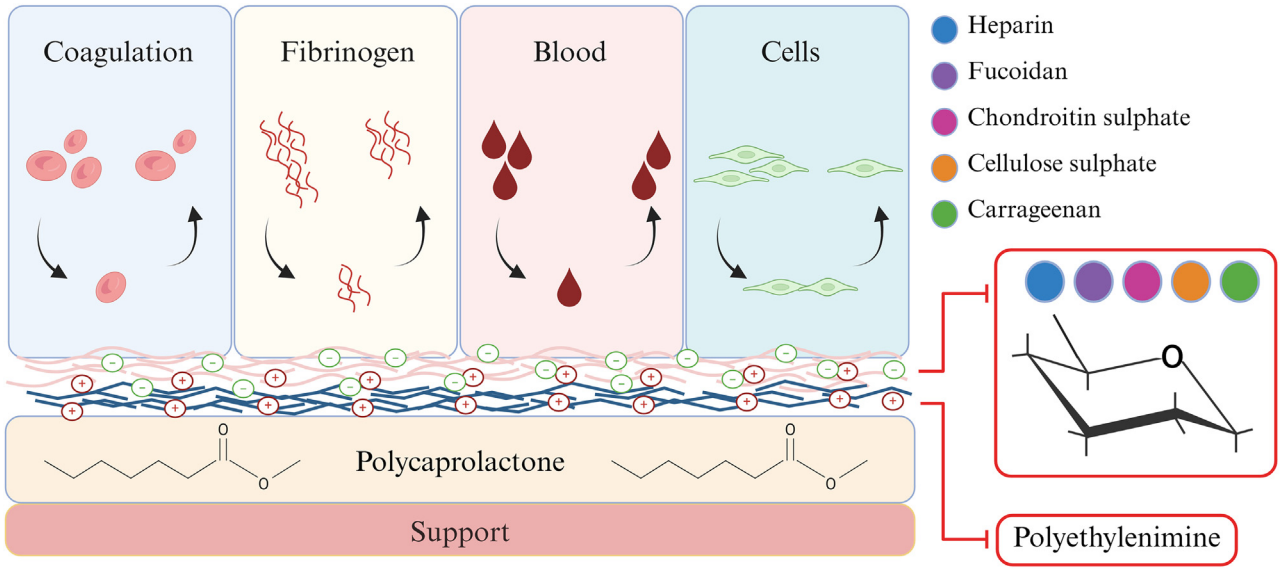

Figure 2. Schematic representation of the non-destructive surface modification of PEI-coated polycarprolactone thin films with an aqueous solution of sulfated polysaccharides and their protein-repellent and cell-adhesive properties

as molecular weight can influence solubility and thus adsorption. Interestingly, the Carr, which had the same amount of total charges (carboxyl and sulfate groups) and molecular weight compared to CS, exhibited lower adsorption. Both CS and Carr are linear SPS, but they differ significantly in their chemical structure.[41] The structural conformation of CS may allow better exposure of the charged groups, whereas the structure of Carr may have steric hindrances that limit its ability to interact with PE, and thus adsorption.

The ΔD_3 followed the trend of the Δf_3 for all polymers (Figure 3B). In addition, the differences in the ΔD_3 for the differently charged SPS during adsorption can be clearly seen, indicating a strong influence of water uptake on the Δf_3 values. This can be further understood from the ΔD_3 values, which means that a higher ΔD_3 favors the formation of a soft and viscous layer. All polymers showed the formation of a viscoelastic layer with higher ΔD_3 ($<2.0 \times 10^{-6}$) during adsorption. Interestingly, CellS ($11.1 \pm 2.3 \times 10^{-6}$) exhibited a 3-fold higher ΔD_3 when compared to Hep ($2.0 \pm 1.1 \times 10^{-6}$), implying that the adsorbed layers of CellS are softer and more viscous. After rinsing the adsorbed layers with NaCl and water, a strong reduction of ΔD_3 was observed. More importantly, the value of ΔD_3 reached almost zero for Carr and was below zero for all other surfaces, suggesting that the loosely bound materials were removed, and a tight and rigid layer was formed. This can be further understood from the slope of the ΔD_3 vs. Δf_3 plot (Figure 3D), which can give further information about the structural properties, hydration and adsorption kinetics of the adsorbed polymers. For example, a higher $\Delta D_3/\Delta f_3$ value indicates a soft and dissipative layer, whereas a lower $\Delta D_3/\Delta f_3$ value is a characteristic of a thin and rigid system.[28,42] For clarity, only the adsorption step is shown in Figure 3D. A complete ΔD_3 vs. Δf_3 plot with the adsorption and rinsing steps is shown in Figure S2. All SPS, with the exception for CS, showed a relatively continuous curve, demonstrating a rather slow adsorption. The slope of $\Delta D_3/\Delta f_3$ is steeper for Carr and CellS compared to Fu and Hep during the adsorption process. This demonstrates that both Carr and CellS were adsorbed in a softer, diffuse conformation and the absorbed layers were more loosely packed and strongly hydrated. Moreover, both Carr and CellS showed more or less the same slope, implying that the adsorbed layers possess the same conformation and viscoelastic properties. Similar behavior was also observed for Fu and Hep, but the adsorbed mass was 4-fold higher (Figure 3B). It can be stated that the adsorbed Fu does not change its conformation or undergo structural rearrangement when the adsorbed mass increases. Interestingly, in the case of CS, the slope of $\Delta D_3/\Delta f_3$ was not constant as adsorption progressed, demonstrating the change in conformation of the adsorbed CS. For all systems, the slope showed a nonlinear behavior after rinsing with NaCl and MilliQ-water (see Figure S2). This can be related to changes in the structural conformation and viscoelastic properties of the adsorbed polymers due to swelling.[30,43] Overall, it can be stated that, all systems formed a more swollen or hydrated layer with loosely packed materials during the adsorption phase, followed by a tightly bound layer with less incorporated water after the rinsing phase.

To determine the water content (Γ_{water}) within the different adsorbed layers, we performed QCM-D D_2O/H_2O exchange studies (Figures 4D and 4E). The SPS coated films showed a higher water content (61–72 Hz, 28.1–131.2 mg m^{-2}) than the uncoated P film (53.2 Hz, 9.4 mg m^{-2}). It was also found that the water content of the coated layers was increased to 20–44% compared to the uncoated P film. The CS, Fu, or Carr coated layers, exhibiting a higher film thickness, showed an increased water content than the Hep or CellS layers. This is in good correlation with the QCM-D results (Figure 3), which showed a higher adsorbed mass for the less SPS (CS to Carr). In general, the increase in water content can be related to the hydration of the hydrophilic and charged groups (e.g.,: $-SO_3H$, $-NH_2$, $-COOH$, and $-OH$) in the SPS coatings. Such coated functional layers on the P film with a higher water content or hydration capacity are beneficial to prevent the unspecific adsorption of proteins (see in the further section).

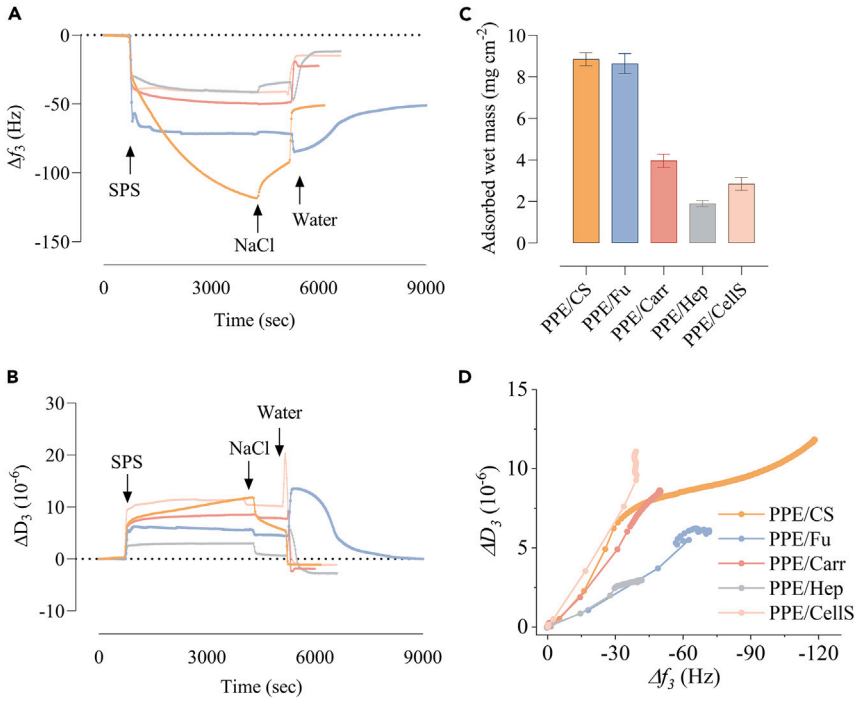

Figure 3. Adsorption of SPS on cationic PE and uncoated P films

QCM-D frequency (A: Δf_3, *a*) and dissipation (B: ΔD_3) change, adsorbed wet mass (C: mg cm^{-2}) and $\Delta f_3/\Delta D_3$ *plot* (D) for the adsorption of sulfated polysaccharides (at c = 0.2 wt. %, in 150 mM NaCl, pH 7.4, Q = 0.1 mL min^{-1}, *n* = 4) on the PE coated P films.

See also Figures S1 and S2. The values in Figure 3C are presented in as ± SD.

Morphology, wettability, thickness, composition, and charges of the coatings

We also characterized the surface properties of the P thin films before and after functionalization with SPS. Functionalization with SPS changed the morphology and roughness of the uncoated P film (see Figure 4). Compared to Carr and CellS, all other coatings showed a more particle-like morphology. This is more pronounced for Fu, CS, and Hep. More open and core-shell structures were observed for CellS, indicating that CellS organized differently on the surface during the adsorption process. The surface roughness of the P film increased considerably from 4.2 to 76.4 nm, which was more pronounced for Hep and CellS coated surfaces. As expected, the layer thickness of the uncoated P films (51.0 ± 1.0 nm) increased with increasing QCM-D adsorbed mass, with a maximum of 134.4 ± 7.8 nm for CS and 86.0 ± 10.4 nm and 80.1 ± 15.2 nm for Hep and CellS coatings, respectively. We also evaluated the stability of SPS coatings by incubating them in an endothelial (EGM-2) culture medium at 37°C for 24 h under simulated unidirectional flow conditions using QCM-D. The stability of the coatings was continuously monitored in real time, as shown in Figure S3. The results indicated that the EGM-2 medium, which contains FBS, was absorbed in varying amounts on all surfaces during the adsorption phase, with partial desorption occurring upon rinsing with water. This observation suggests that the SPS coating remained intact despite the adsorption of EGM-2, demonstrating the coating's stability. As expected, the XPS measurements (Figure 4C) revealed the presence of sulfur atoms (at.%) for all SPS coated surfaces. The Hep and CellS, coatings had a higher sulfur content than the other coatings. This is consistent with the overall charge density of the polymers (see Table 1). According to the static water contact angle SCA(H_2O) measurements, the uncoated P film was changed from hydrophobic (SCA(H_2O): 90.2 ± 1.4°) to moderately hydrophilic with an SCA(H_2O) of 60–70° after functionalization with SPS. pH-dependent surface zeta potential was also measured to determine the effect of the coatings on the overall surface charge of the films. As can be seen in Figures 4F and 4G, all coated films exhibited negative zeta potential values of −40 to −50 mV (pH: 7–9). This is 10–20 mV higher than the uncoated P films (−30 mV) indicating a strong contribution of the sulfates to the surface charge of the films. The PPE films exhibited a high cationic charge of 22 mV (at pH = 2, Figure S4), which was not observed for the SPS coated surfaces, indicating that the underlying PPE surfaces were fully covered and did not affect the surface properties of the coated films. This can be further confirmed by the decrease in the isoelectric point (IEP) from 4.5 for PPE to 3.0 < IEP <3.5 for the SPS. All these results (Figure 3) confirm that the P film was successfully functionalized with the antithrombogenic SPS.

In-vitro hemocompatibility and fibrin adsorption

Anticoagulant studies by QCM-D

Although APTT values provide important information about the anticoagulant effect, i.e., the total coagulation time of SPS in solution, there are at least two other important aspects that should be considered when it comes to the use of such materials as coatings in contact with living

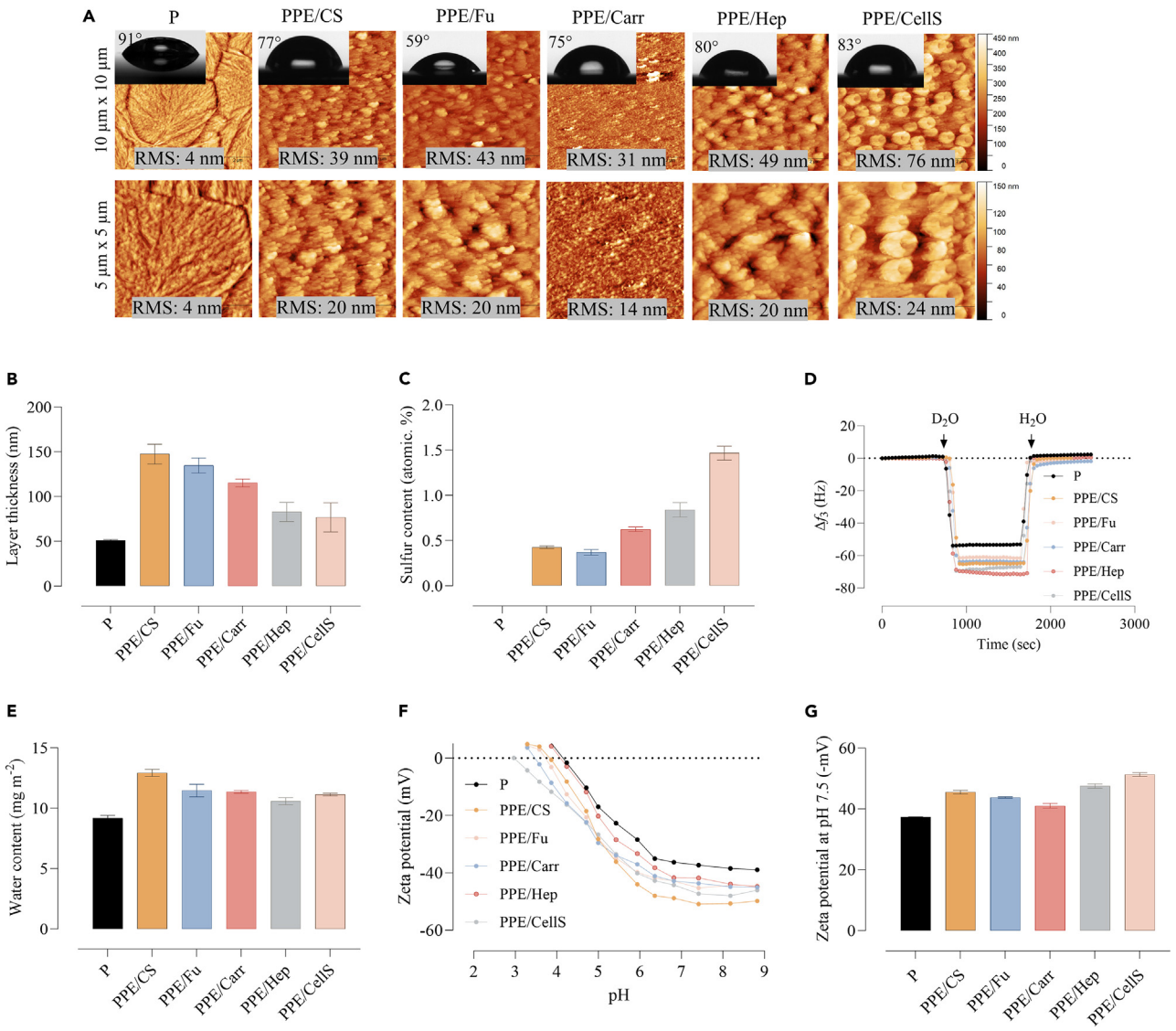

Figure 4. SPS coating characterization

AFM height images (A), profilometry thickness (B), sulfur content by XPS (C) change in Δf_3 for the D_2O/H_2O exchange (D), water content calculated from the D_2O/H_2O exchange (E), surface zeta potential (F and G) of P thin films before and after functionalization with PE and SPS (n = 3), and values are presented as ± SD. See also Figures S3 and S4.

tissue. These include the anticoagulant effect of SPS coated surfaces and their interactions with living cells. Both aspects are discussed in the futher section.

The anticoagulant activity of coated surfaces was studied in real-time using QCM-D.[14,17–19,29,44] In this case, the coated QCM-D sensors were mounted in an open measurement cell to which the APTT reagents were manually added. This adopted APTT test was performed in the same way as the standard test. A measurement with the P and PPE coated QCM-D sensors was performed as a reference to estimate the influence of SPS coating on the coagulation process. The adopted APTT test with the QCM-D A provides information about the kinetics of blood clotting, the viscoelastic properties (e.g., clot density), and the time of onset and rate of fibrin deposition.[18,45] As can be seen in Figure 5A, once the coagulation cascade was initiated by the addition of $CaCl_2$ at ~2 min, the Δf_3 remained rather stable for all surfaces for about 7 min, indicating the formation of thrombin from prothrombin.[14,19,29,31] Afterward, a major reduction of Δf_3 was observed, which can be related to the formation of fibrin fibers that form a clot and deposit on the surface. Following this, stabilization of Δf_3 was observed, indicating the completion of coagulation process. The latter step can be used to determine the endpoint of total coagulation. However, the stabilization of Δf_3 was often difficult to determine, so the stabilization of ΔD_3 (Figure 5B) was used as it was more pronounced. The ΔD_3 during clot formation followed a similar trend to the Δf_3. After the initiation of the coagulation cascade, ΔD_3 remained rather stable and started to

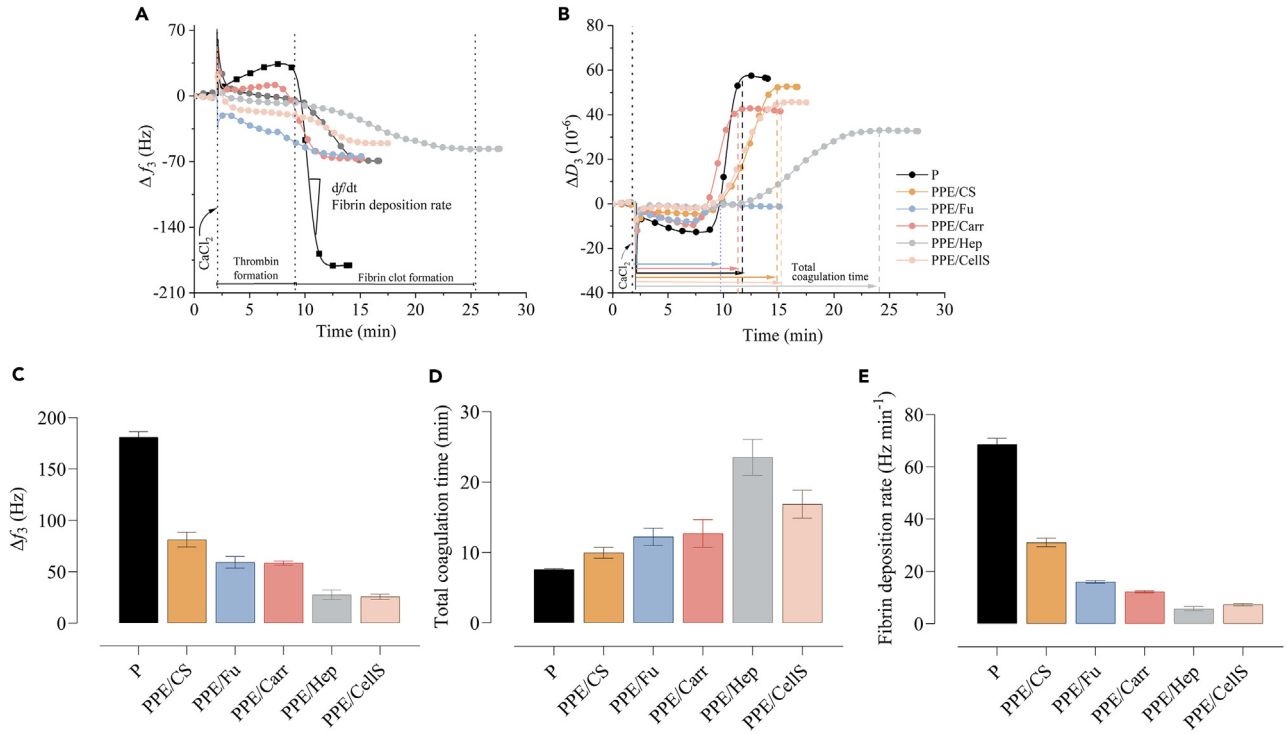

Figure 5. Clot formation by QCM-D on P thin films coated with SPS

QCM-D change in Δf_3 (A) and ΔD_3 (B) during clot formation, total change in Δf_3 (C), total coagulation time (D) and fibrin deposition rate of P thin films coated with SPS (E) (n = 4), and values are presented as ± SD. See also Figure S5.

increase after the fibrin clot was formed. This indicates that the increase in elasticity of the liquid above the quartz crystal to a point of high viscoelasticity, which dampens the oscillation.[19,29,31,33] After the coagulation process ended, the ΔD_3 was stable and no further changes in elasticity were observed.

Figure 5C shows that the Δf_3 (deposition of fibrin) and the total coagulation times vary largely for the coatings prepared using different SPS. Compared to the uncoated P surfaces, a substantially lower Δf_3 was observed for all coated surfaces. This implies that the sulfate groups present on the surfaces suppressed the fibrin fiber formation and deposition. We also tested the anticoagulation activity of PPE surfaces. It was found that the Δf_3 decreased from 181.3 ± 6.5 Hz for the neat P to 130.4 ± 5.6 Hz for the cationic PE coated surfaces (see Figure S4). An explanation for this could be that the PE molecules blocked the interaction between fibrinogen and thrombin, leading to inhibition of fibrin formation.[19,46] In general, the Δf_3 decreased with increasing sulfate content of the polysaccharide. The CellS, which had a higher sulfate content (1.5 ± 0.1 at%), showed a lower reduction in Δf_3 (26 ± 3 Hz) compared to other coated surfaces. Similar results were obtained for Hep (Δf_3: 28 ± 5 Hz), a known anticoagulant with a sulfate content of 0.8 ± 0.1 at%. The reduction of Δf_3 is comparable and no statistical differences were found for the other three SPS (CS, Fu and Carr), which exhibited almost similar sulfate content (see Figure 4F). It seems that the fibrin deposition rate (Figure 5E) depends to some extent on the amount of sulfate functional groups as well as on the Δf_3/min values. The latter dropped from 31.5 ± 2.0 Hz/min for CS (0.4 ± 0.01 at% S) to 5.9 ± 1.0 Hz/min for Hep (0.8 ± 0.1 at% S). CellS and Hep outperformed other coated surfaces. The performance of SPS in terms of fibrin deposition rate is as follows: CS < Fu < Carr < CellS < Hep. Figure 5D shows that all SPS coated surfaces prolonged the coagulation time compared to uncoated P (over 36% for CS and over 198% for Hep), indicating that the coagulation cascade develops slowly on the surfaces coated with selected SPS. The total coagulation time increased with increasing amount of sulfate content of the PS. For example, the total coagulation time for CS increased from 10.2 ± 0.2 min to 22.4 ± 0.7 min for Hep. Interestingly, the CellS showed a shorter coagulation time than Hep but outperformed all other coatings. The overall performance of SPS in terms of total coagulation time is as follows: CS < Fu < Carr < CellS < Hep. Studies have shown that the SPS used can enhance the hemocompatibility of the materials through multiple mechanisms. These SPS mimic the natural anticoagulant properties of the endothelial glycocalyx, reducing platelet adhesion and activation.[26,27] The SPS also interact with plasma proteins, modulating the protein adsorption profile to favor antithrombogenic effects. Additionally, SPS coated surfaces can inhibit the coagulation cascade by potentiating antithrombin activity, thereby preventing thrombus formation.[47] This inhibition is attributed to the highly negatively charged sulfate groups, which repels negatively charged blood components and reduces unspecific protein adsorption, leading to improved hemocompatibility.[48,49] Detailed studies using various characterization techniques and blood compatibility experiments performed in this work supported these findings, demonstrating the efficacy of SPS in enhancing the blood compatibility of PCL.

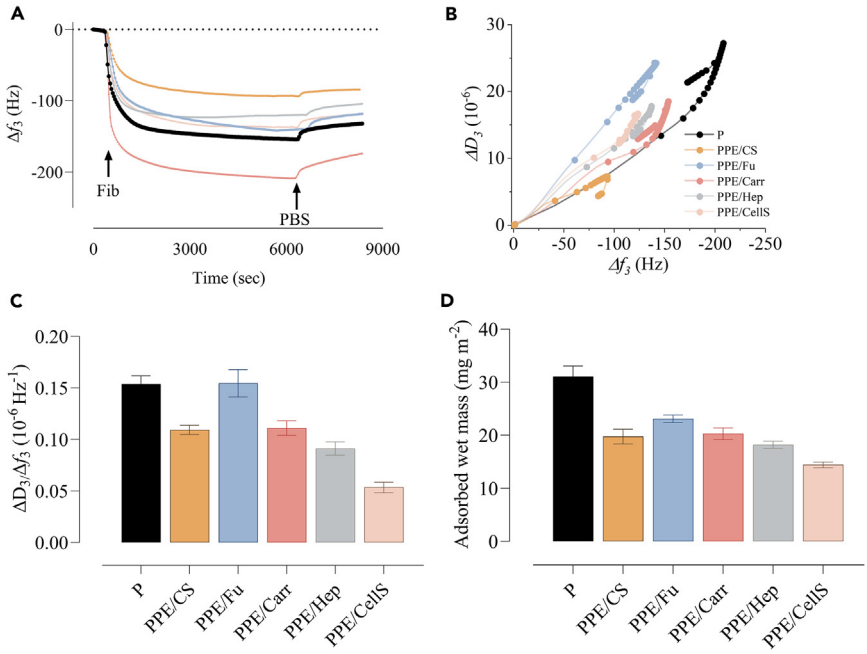

Figure 6. Fibrinogen adsorption (c = 3 mg mL^{-1}, pH 7.4) on uncoated and SPS coated P thin films

(A) changes in frequency, (B) $\Delta f_3/\Delta D_3$ plot, (C) adsorbed mass, and (D) $\Delta f_3/\Delta D_3$ ratio determined for the adsorption of Fib on the uncoated and SPS coated PS surfaces (n = 3), and values are presented as ± SD.

Establishing the anticoagulative activity of SPS on solid surfaces is an important step toward understanding their impact when used as coatings for medical implants. But another piece of the puzzle to evaluate their performance in living tissue is the behavior of cells when they come into contact with such coatings. Therefore, the response of ECs to the coatings was studied in further detail (discussed in futher section).

Fibrinogen adsorption

We selected fibrinogen (Fib) as our model protein primarily because of its well-documented role in the extensive inspection adsorption and subsequent development of surface-induced thrombosis.[50,51] Although other proteins such as bovine serum albumin (BSA) and gamma-globulin (γ-GL) can play significant roles in surface-induced thrombosis and overall protein adsorption profiles,[17,30] Fib is a key player in clot formation, directly influencing platelet adhesion and activation, which are critical factors in thrombogenesis.[52,53] Therefore, it is important to understand the adsorption behavior of Fib on P surfaces before and after coating with SPS. Figure 6A shows the typical QCM-D results obtained for the adsorption of Fib on the uncoated and SPS functionalized P thin films. Once the Fib was introduced into the QCM flow cell, a rapid reduction in Δf_3 (Figure 6A) followed by saturation of the surfaces was observed. This indicates a strong interaction of the Fib molecules to the adsorbing surfaces. After rinsing with PBS buffer, a minor increase in Δf_3 was noted, which can be due to the removal of loosely bound Fib molecules from the surface. As expected, the uncoated P films showed a maximum deposition of Fib (Δf_3 = −175.4 ± 5.4 Hz, Figure 6A, 31.1 ± 2.2 mg m^{-2}; Figure 6C) compared to all other surfaces. This can be explained by the high hydrophobicity of P (SCA(H_2O) of 91 ± 0.6°), which favor the irreversible adsorption of Fib, mainly due to physical interactions such as hydrophobic, van der Waals and H-bonds.[28,54,55] All SPS coatings, except CS, did not show much difference in Fib adsorption. For example, CS (charge titration: SO_4^{2-}: 3 mmol g^{-1}, COOH: 1.3 mmol g^{-1}; XPS: 0.43 ± 0.02 atm%), which has a lower sulfate content, showed less Fib adsorption (Δf_3 = −118.5 ± 5.4 Hz, Figure 3A, 19.8 ± 1.9 mg m^{-2}; Figure 6C) when compared with Fu (QCM-D: Δf_3 = −132.2 ± 6.4 Hz, 23.1 ± 0.7 mg m^{-2}; charge titration: SO_4^{2-}: 3.9 ± 0.1 mmol g^{-1}; XPS: Figure 4C) or Carr (QCM-D: Δf_3 = −119.7 ± 7.8 Hz, 20.3 ± 1.1 mg m^{-2}; charge titration: SO_4^{2-}: 4.2 mmol g^{-1}; XPS: 0.62 ± 0.03%). It is assumed that the presence of carboxyl groups in addition to sulfate groups in CS contribute to less Fib adsorption. Interestingly, Hep (charge titration: SO_4^{2-}: 4.4 ± 0.1 mmol g^{-1}, COOH: 1.4 ± 0.1 mmol g^{-1}, XPS: 0.84%), with 32% and 7% more sulfate and carboxyl groups than CS showed more Fib adsorption (Δf_3 = −104.6 ± 3.4 Hz, 18.2 ± 0.7 mg m^{-2}). It should be noted that the total charge and sulfate content are higher in Hep is higher compared to CS. The CellS, with the highest sulfate content (charge titration: SO_4^{2-}: 7.0 ± 0.3 mmol g^{-1}, XPS: 1.5 ± 0.1%) also showed more Fib adsorption (Δf_3 = −84.2 ± 4.5 Hz, 14.5 ± 0.5 mg m^{-2}) than the CS-coated surfaces. Overall, the following trend was observed for the Fib adsorption (see Figure 6C): P > Fu > CellS > Carr > Hep > CS. The $\Delta f_3/\Delta D_3$ plot for adsorption of Fib on the SPS coated surfaces is shown in Figure 6B. Changes in the slope of the $\Delta f_3/\Delta D_3$ plot or variations in the ΔD_3 value can be observed for all samples. This indicates changes in the elasticity of the adsorbed layer due to a change in the conformation of the Fib. The nature of the slope of the $\Delta f_3/\Delta D_3$ graph allows us to interpret the conformational changes of the Fib and the viscoelasticity of the adsorbed layer. An increase in ΔD_3 or a higher slope can be related to viscous/hydrated layer with "end-on" or an extended conformation

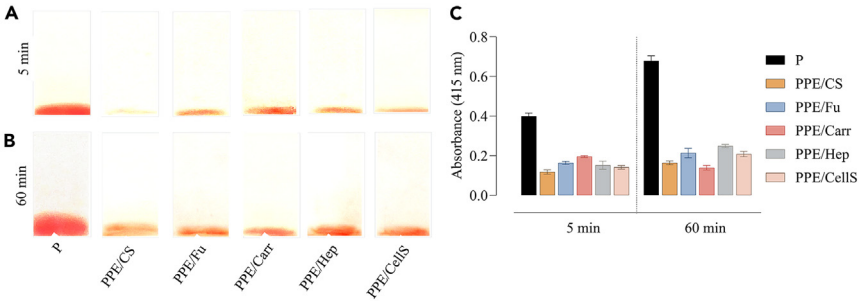

Figure 7. Human blood compatibility of uncoated and sulfated polysaccharide coated P thin films

Photographs of uncoated and sulfated polysaccharide coated P thin films (or foils) removed from whole blood after 5 min (A) and 60 min (B) immersion. (C) Absorbance values measured for uncoated and sulfated polysaccharide coated polycaprolactone thin films (or foils) after incubation and rinsing (5 and 60 min) with human whole blood (n = 4), and values are presented as ± SD.

of Fib, whereas "side-on" and a compact conformation can lead to decrease in dissipation energy, due to the more rigid nature of the formed layer.[28,56] As shown in Figure 6B, except CS, all other coated surfaces exhibited an increased slope and ΔD_3 during the adsorption process. This was also observed for the uncoated P surfaces. This implies that the Fib molecules were adsorbed in an extended or "end-on" confirmation on all these surfaces. In the case of CS, a lower slope and ΔD_3 was observed, suggesting that a more right or compact structure with "side-on" conformation was formed during the adsorption of Fib.

Obviously, the negatively charged SPS coated surfaces strongly repelled the Fib adsorption compared to neat hydrophobic P surfaces. Fib is hydrophobic, large, and rich in deprotonated carboxyl groups (−0.31 mmol g^{-1}) at pH 7.[17,28] This explains the increased deposition of Fib (at pH 7.4, isoelectric point: 5.2) on the uncoated P surfaces. It is suggested that the strong protein repellent capacity of the SPS coated surfaces is due to the electrostatic repulsion between the negatively charged groups of the Fib and the charged groups of the PS, in addition to the hydration forces. The presence of different hydrophilic and charged functional groups (such as −OH, −CONH, −COOH, SO_4^{2-}) in SPS can contribute to increased hydration of the coated layer. In addition, these functional groups act as H-bond donor or acceptor and create repulsive steric forces, so that they can intercalate larger amounts of water via electrostatically induced hydration and H-bond interactions.[57,58] Thus, the highly hydrated layer can lead to maximum protein rejection. The information about the surface hydration can be obtained from $\Delta D_3/\Delta f_3$ ratio (Figure 6D), meaning that the layer with a high $\Delta D_3/\Delta f_3$ ratio is considered to be highly hydrated or viscoelastic. According to Figure 6D, the CS coated surfaces showed a maximum $\Delta D_3/\Delta f_3$ ratio of 0.18 than the other coated and uncoated and P surfaces. This implies that the CS layers were highly hydrated and thus increased the repulsion and reduced deposition of Fib. This is also in good correlation with D_2O/H_2O exchange studies, where the highest water content was determined for the CS layers.

Whole blood adhesion

Figure 7 shows photos of the uncoated and SPS coated P films immersed in whole blood for 5 min (Figure 7A) and 60 min (Figure 7B). It shows a higher blood adhesion on the uncoated P film, whereas all coated films showed a lower blood adhesion. For all tested samples, higher blood adhesion can be observed at 60 min immersion compared to 5 min. Although the samples immersed for 5 min showed differences in blood adhesion, the differences between each polysaccharide coating are no longer visible in the photos after 60 min. The absorbance (at 415 nm) of the released hemoglobin after rinsing the samples shows a clearer picture and reveals a decrease in absorbance (5 min test) from 0.4 for uncoated P films to 0.12, 0.16, 0.19, 0.15, 0.14, for PPE/CellS, PPE/Fu, PPE/Carr, PPE/CS, and PPE/Hep, respectively. For the 60 min test, the trend of absorbance follows the same trend as absorbance decreased from 0.7 for the uncoated P film to 0.16, 0.21, 0.14, 0.24, 0.21, for PPE/CellS, PPE/Fu, PPE/Carr, PPE/CS, and PPE/Hep, respectively. The results show that the less SPS such as CS or Carr can effectively reduce blood adhesion compared to the highly sulfated ones such as Hep or CellS. This can be due to the higher water content or hydration capacity of the coated layers, which effectively reduced the adhesion of whole blood.

Endothelial cell response to the coatings

According to the results of number EC adhesion visualized with DAPI staining (Figure 8A) showed cell attachment on all surfaces. The images showed that a large population of hECs adhered to the CS-coated surfaces compared to all other coated and uncoated P surfaces. This observation was further supported by the cell density results (Figure 8B). The number of cells adhering to the CS-coated surfaces was found to be statistically different from the uncoated P films. Similar trends were observed for Fu- and Carr-coated surfaces. In contrast, the two other highly SPS coatings such as Hep and Cell were comparable to the uncoated P films. In addition, the CS and Hep coated surfaces exhibited a significantly larger cell coverage area compared to uncoated P surfaces (Figure 8C). However, differences were observed for circularity (Figure 8D) only with FU-, Carr- and CellS-coating compared to uncoated P surface. Overall, the hECs adhered to all coated surfaces in a more spread conformation compared to uncoated P films. The hECs grew for 24 h on either uncoated or SPS-coated P surfaces and were evaluated for viability (Figure 9), which showed no statistical differences and was comparable between all coated surfaces. This indicates that the formation of a biocompatible SPS layer favoring endothelial cell growth and adherence was effectively supported.

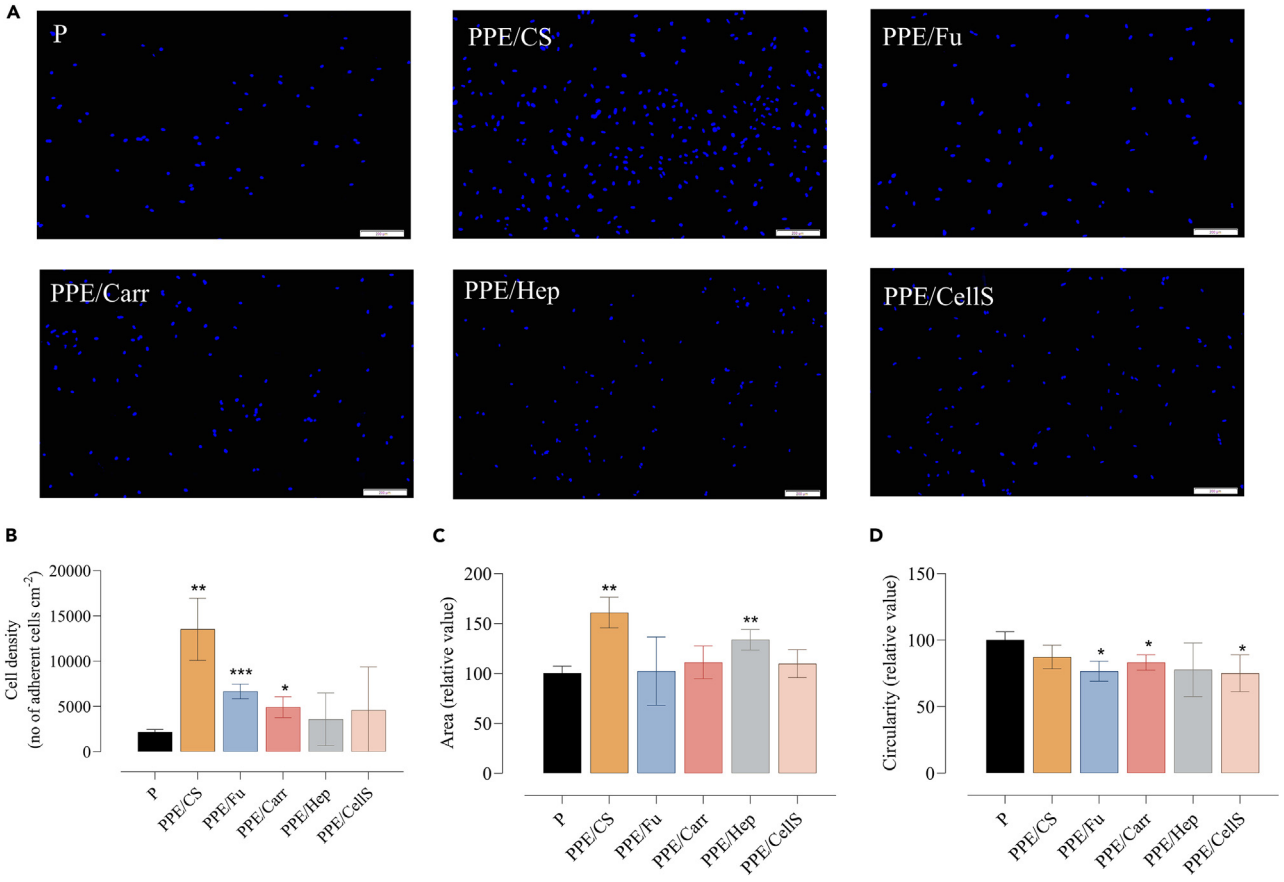

Figure 8. Adhesion characteristics of human primary endothelial cells on uncoated and sulfated polysaccharide coated polycaprolactone surfaces

(A) DAPI staining of the surfaces on 6 h after (hECs) cell culture (n = 3). Cell density (B), area (C), and circularity (D) of hECs on uncoated and SPS coated surfaces determined after 6 h of culture (n = 3). The Student's t test was used for statistical analysis, and values are presented as ± SD. *p values <0.05, **p values <0.001, ***p values <0.001 were considered statistically significant.

Overall, in this study, we have presented an aqueous method for modifying the surfaces of polycaprolactone biomaterials with various SPS. The surface modification of polycaprolactone was performed by first coating polyethylenimine and then SPS such as CS, fucoidan, carrageenan, heparin, and cellulose sulfate via an electrostatic interaction. This was carried out by QCM-D adsorption experiments and dip coating. The functional coatings with different SPS changed the surface properties of polycaprolactone in terms of morphology, charges, wettability, thickness, and roughness. The less charged PS (CS and fucoidan) showed higher mass deposition compared to other SPS, as shown by the QCM-D results. Functionalization with SPS increased the layer thickness while increasing the water content, as shown by profilometry and D_2O/H_2O studies. Atomic force microscopy showed a particle-like structure with a rougher morphology in all coated samples. The wettability of the polycaprolactone surfaces was also reduced from 91° (hydrophobic) to 59° (moderately hydrophilic). The successful functionalization of the P surfaces was also evidenced by the increase in the negative zeta potential of the surface and the emergence of sulfate content. The QCM-D coagulation experiments showed low fibrin deposition and longer clotting time for heparin and cellulose sulfate compared to other SPS, the less sulfated ones. In general, all sulfated polysaccharide coatings showed excellent anticoagulant activity (low fibrin deposition) compared to uncoated polycaprolactone. This was also shown for human fibrinogen and whole blood adhesion, with the uncoated polycaprolactone showing more fibrinogen and blood adhesion and the coated surfaces showing 30–40% less fibrinogen deposition and more than 50% less whole blood adhesion. The cell assay experiments showed that the human endothelial cells adhered to both uncoated and sulfated polysaccharide surfaces in viable form, but more cells adhered to the coated CS surfaces. In conclusion, the functional coatings of antithrombogenic PS on polyester vascular grafts provide a multifaceted approach to improve graft performance by enhancing hemocompatibility, repelling proteins, and promoting a favorable endothelial cell response, ultimately contributing to better patient outcomes in vascular surgery.

Limitation of the study

The less SPS such as CS or carrageenan showed excellent repellent capacity against fibrinogen protein and whole blood. We focused here only on fibrinogen due to its direct and significant impact on thrombus formation. However, other proteins, such as bovine serum albumin

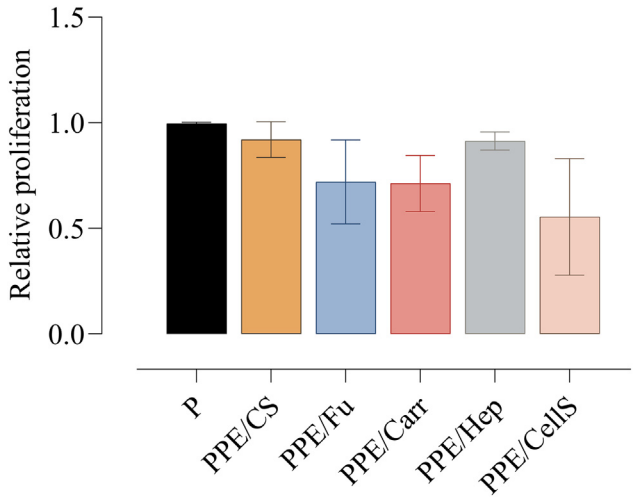

Figure 9. Viability of endothelial cells cultured on different sulfated polysaccharide coated surfaces (n = 3), and values are presented as ± SD

(BSA) and gamma-globulin (γ-GL), also play significant roles in surface-induced thrombosis and overall protein adsorption profiles, but this was not performed in the scope of this study. The anticoagulant activity of less SPS was not improved compared to highly SPS such as heparin or cellulose sulfate. In addition to examining the endothelial inflammatory response, this study lacks *in vivo* experiments with suitable animal models, which are necessary to better understand thrombosis formation and the endothelialization of sulfated polysaccharide coatings.

STAR★METHODS

Detailed methods are provided in the online version of this paper and include the following:

- KEY RESOURCES TABLE
- RESOURCE AVAILABILITY
  - Lead contact
  - Materials availability
  - Data and code availability
- EXPERIMENTAL MODEL AND STUDY PARTICIPANT DETAILS
  - Cell lines
- METHOD DETAILS
  - General material details
  - Cellulose sufate synthesis
  - pH-potentiometric titration
  - Polyelectrolyte titration
  - Sample preparation
  - *In-vitro* hemocompatibility evaluation
  - Preparation of polycaprolactone (P) thin films
  - Quartz crystal microbalance with dissipation (QCM-D)
  - Functionalization of polycaprolactone (P) thin films with sulphated PS
  - Adsorption of endothelial cell culture medium-2
  - D_2O/H_2O exchange studies
  - Adsorption of fibrinogen (Fib)
  - Clotting formation and time determination
  - Whole blood adhesion
  - Cell culture
  - Cell adhesion and viablity
  - Description of cellular morphology
  - Surface analytics
- QUANTIFICATION AND STATISTICAL ANALYSIS

SUPPLEMENTAL INFORMATION

Supplemental information can be found online at https://doi.org/10.1016/j.isci.2024.110692.

ACKNOWLEDGMENTS

The authors acknowledge the financial support received from the Slovenian Research Agency (grant. no: P2-0118, J1-4416, and J4-1764).

AUTHOR CONTRIBUTIONS

Conceptualization and methodology, M.B. and T.M.; formal analysis, M.B., F.L., O.P., R.C.F., A.O., K.S.K., and C.N.; investigation, M.B., F.L., O.P., R.C.F., T.H., and C.N.; writing-original draft, M.B., C.N., and T.M.; writing-review and editing, M.B., A.O., K.S.K., C.N., and T.M.; visualization, M.B., F.L., C.N., and T.M.; supervision, T.M.

DECLARATION OF INTERESTS

The authors declare no competing interests.

Received: March 25, 2024
Revised: June 5, 2024
Accepted: August 5, 2024
Published: August 12, 2024

REFERENCES

1. Jaffer, I.H., and Weitz, J.I. (2019). The blood compatibility challenge. Part 1: Blood-contacting medical devices: The scope of the problem. Acta Biomater. *94*, 2–10. https://doi.org/10.1016/j.actbio.2019.06.021.
2. Hong, J.K., Gao, L., Singh, J., Goh, T., Ruhoff, A.M., Neto, C., and Waterhouse, A. (2020). Evaluating medical device and material thrombosis under flow: current and emerging technologies. Biomater. Sci. *8*, 5824–5845. https://doi.org/10.1039/D0BM01284J.
3. Chen, J., Zhang, D., Wu, L.-P., and Zhao, M. (2023). Current Strategies for Engineered Vascular Grafts and Vascularized Tissue Engineering. Polymers *15*, 2015.
4. Ravi, S., and Chaikof, E.L. (2010). Biomaterials for vascular tissue engineering. Regen. Med. *5*, 107–120. https://doi.org/10.2217/rme.09.77.
5. Leal, B.B.J., Wakabayashi, N., Oyama, K., Kamiya, H., Braghirolli, D.I., and Pranke, P. (2020). Vascular Tissue Engineering: Polymers and Methodologies for Small Caliber Vascular Grafts. Front. Cardiovasc. Med. *7*, 592361. https://doi.org/10.3389/fcvm.2020.592361.
6. Vesel, A., Zaplotnik, R., Primc, G., Mozetič, M., Katan, T., Kargl, R., Mohan, T., and Kleinschek, K.S. (2021). Non-Equilibrium Plasma Methods for Tailoring Surface Properties of Polyvinylidene Fluoride: Review and Challenges. Polymers *13*, 4243.
7. Zizhou, R., Wang, X., and Houshyar, S. (2022). Review of Polymeric Biomimetic Small-Diameter Vascular Grafts to Tackle Intimal Hyperplasia. ACS Omega *7*, 22125–22148. https://doi.org/10.1021/acsomega.2c01740.
8. Pan, Y., Zhou, X., Wei, Y., Zhang, Q., Wang, T., Zhu, M., Li, W., Huang, R., Liu, R., Chen, J., et al. (2017). Small-diameter hybrid vascular grafts composed of polycaprolactone and polydioxanone fibers. Sci. Rep. *7*, 3615. https://doi.org/10.1038/s41598-017-03851-1.
9. Park, S., Kim, J., Lee, M.-K., Park, C., Jung, H.-D., Kim, H.-E., and Jang, T.-S. (2019). Fabrication of strong, bioactive vascular grafts with PCL/collagen and PCL/silica bilayers for small-diameter vascular applications. Mater. Des. *181*, 108079. https://doi.org/10.1016/j.matdes.2019.108079.
10. Gong, W., Lei, D., Li, S., Huang, P., Qi, Q., Sun, Y., Zhang, Y., Wang, Z., You, Z., Ye, X., and Zhao, Q. (2016). Hybrid small-diameter vascular grafts: Anti-expansion effect of electrospun poly ε-caprolactone on heparin-coated decellularized matrices. Biomaterials *76*, 359–370. https://doi.org/10.1016/j.biomaterials.2015.10.066.
11. Zhu, Y., Mao, Z., and Gao, C. (2013). Aminolysis-based surface modification of polyesters for biomedical applications. RSC Adv. *3*, 2509–2519. https://doi.org/10.1039/C2RA22358A.
12. Ishihara, K. (2019). Blood-Compatible Surfaces with Phosphorylcholine-Based Polymers for Cardiovascular Medical Devices. Langmuir *35*, 1778–1787. https://doi.org/10.1021/acs.langmuir.8b01565.
13. Ozaltin, K., Lehocky, M., Humpolicek, P., Pelkova, J., Di Martino, A., Karakurt, I., and Saha, P. (2019). Anticoagulant Polyethylene Terephthalate Surface by Plasma-Mediated Fucoidan Immobilization. Polymers *11*, 750.
14. Gericke, M., Doliška, A., Stana, J., Liebert, T., Heinze, T., and Stana-Kleinschek, K. (2011). Semi-Synthetic Polysaccharide Sulfates as Anticoagulant Coatings for PET, 1 – Cellulose Sulfate. Macromol. Biosci. *11*, 549–556. https://doi.org/10.1002/mabi.201000419.
15. Liu, Y., He, T., and Gao, C. (2005). Surface modification of poly(ethylene terephthalate) via hydrolysis and layer-by-layer assembly of chitosan and chondroitin sulfate to construct cytocompatible layer for human endothelial cells. Colloids Surf. B Biointerfaces *46*, 117–126. https://doi.org/10.1016/j.colsurfb.2005.09.005.
16. Obiweluozor, F.O., Emechebe, G.A., Kim, D.-W., Cho, H.-J., Park, C.H., Kim, C.S., and Jeong, I.S. (2020). Considerations in the Development of Small-Diameter Vascular Graft as an Alternative for Bypass and Reconstructive Surgeries: A Review. Cardiovasc. Eng. Technol. *11*, 495–521. https://doi.org/10.1007/s13239-020-00482-y.
17. Mohan, T., Nagaraj, C., Nagy, B.M., Bračič, M., Maver, U., Olschewski, A., Stana Kleinschek, K., and Kargl, R. (2019). Nano- and Micropatterned Polycaprolactone Cellulose Composite Surfaces with Tunable Protein Adsorption, Fibrin Clot Formation, and Endothelial Cellular Response. Biomacromolecules *20*, 2327–2337. https://doi.org/10.1021/acs.biomac.9b00304.
18. Ehmann, H.M.A., Mohan, T., Koshanskaya, M., Scheicher, S., Breitwieser, D., Ribitsch, V., Stana-Kleinschek, K., and Spirk, S. (2014). Design of anticoagulant surfaces based on cellulose nanocrystals. Chem. Commun. *50*, 13070–13072. https://doi.org/10.1039/C4CC05254D.
19. Bračič, M., Mohan, T., Kargl, R., Grießer, T., Heinze, T., and Stana Kleinschek, K. (2021). Protein repellent anti-coagulative mixed-charged cellulose derivative coatings. Carbohydr. Polym. *254*, 117437. https://doi.org/10.1016/j.carbpol.2020.117437.
20. Barrowcliffe, T.W., Mulloy, B., Johnson, E.A., and Thomas, D.P. (1989). The anticoagulant activity of heparin: Measurement and relationship to chemical structure. J. Pharm. Biomed. Anal. *7*, 217–226. https://doi.org/10.1016/0731-7085(89)80086-X.
21. Goodwin, S.C., Yoon, H.-C., Chen, G., Abdel-Sayed, P., Costantino, M.M., Bonilla, S.M., and Nishimura, E. (2003). Intense Inflammatory Reaction to Heparin Polymer CoatedIntravascular Palmaz Stents in Porcine Arteries Compared to UncoatedPalmaz Stents. Cardiovasc. Intervent. Radiol. *26*, 158–167. https://doi.org/10.1007/s00270-002-2562-0.
22. Hirsh, J., Raschke, R., Warkentin, T.E., Dalen, J.E., Deykin, D., and Poller, L. (1995). Heparin: Mechanism of Action, Pharmacokinetics, Dosing Considerations, Monitoring, Efficacy, and Safety. Chest *108*, 258S–275S. https://doi.org/10.1378/chest.108.4_Supplement.258S.
23. Thalla, P.K., Fadlallah, H., Liberelle, B., Lequoy, P., De Crescenzo, G., Merhi, Y., and Lerouge, S. (2014). Chondroitin Sulfate Coatings Display Low Platelet but High

Endothelial Cell Adhesive Properties Favorable for Vascular Implants. Biomacromolecules *15*, 2512–2520. https://doi.org/10.1021/bm5003762.

24. Wang, X., Hadi, M.K., Niu, J., Zhou, Q., and Ran, F. (2023). Anticoagulant Macromolecules. Macromolecules *56*, 4387–4430. https://doi.org/10.1021/acs.macromol.2c02501.
25. Heestermans, M., Poenou, G., Hamzeh-Cognasse, H., Cognasse, F., and Bertoletti, L. (2022). Anticoagulants: A Short History, Their Mechanism of Action, Pharmacology, and Indications. Cells *11*, 3214.
26. Ciancia, M., Quintana, I., and Cerezo, A.S. (2010). Overview of Anticoagulant Activity of Sulfated Polysaccharides from Seaweeds in Relation to their Structures, Focusing on those of Green Seaweeds. Curr. Med. Chem. *17*, 2503–2529. https://doi.org/10.2174/092986710791556069.
27. Melo, F.R., Pereira, M.S., Foguel, D., and Mourão, P.A.S. (2004). Antithrombin-mediated Anticoagulant Activity of Sulfated Polysaccharides: Different mechanisms for heparin and sulfated galactans. J. Biol. Chem. *279*, 20824–20835. https://doi.org/10.1074/jbc.M308688200.
28. Ajdnik, U., Zemljič, L.F., Plohl, O., Pérez, L., Trček, J., Bračič, M., and Mohan, T. (2021). Bioactive Functional Nanolayers of Chitosan–Lysine Surfactant with Single- and Mixed-Protein-Repellent and Antibiofilm Properties for Medical Implants. ACS Appl. Mater. Interfaces *13*, 23352–23368. https://doi.org/10.1021/acsami.1c01993.
29. Mohan, T., Chirayil, C.J., Nagaraj, C., Bračič, M., Steindorfer, T.A., Krupa, I., Maadeed, M.A.A.A., Kargl, R., Thomas, S., and Stana Kleinschek, K. (2021). Anticoagulant Activity of Cellulose Nanocrystals from Isora Plant Fibers Assembled on Cellulose and SiO_2 Substrates via a Layer-by-Layer Approach. Polymers *13*, 939.
30. Mohan, T., Niegelhell, K., Nagaraj, C., Reishofer, D., Spirk, S., Olschewski, A., Stana Kleinschek, K., and Kargl, R. (2017). Interaction of Tissue Engineering Substrates with Serum Proteins and Its Influence on Human Primary Endothelial Cells. Biomacromolecules *18*, 413–421. https://doi.org/10.1021/acs.biomac.6b01504.
31. Doliška, A., Strnad, S., Stana, J., Martinelli, E., Ribitsch, V., and Stana-Kleinschek, K. (2012). In Vitro Haemocompatibility Evaluation of PET Surfaces Using the Quartz Crystal Microbalance Technique. J. Biomater. Sci. Polym. Ed. *23*, 697–714. https://doi.org/10.1163/092050611X559232.
32. Drozd, N.N., Logvinova, Y.S., Torlopov, M.A., and Udoratina, E.V. (2017). Effect of Sulfation and Molecular Weight on Anticoagulant Activity of Dextran. Bull. Exp. Biol. Med. *162*, 462–465. https://doi.org/10.1007/s10517-017-3640-2.
33. Mohan, T., Čas, A., Bračič, M., Plohl, O., Vesel, A., Rupnik, M., Zemljič, L.F., and Rebol, J. (2019). Highly Protein Repellent and Antiadhesive Polysaccharide Biomaterial Coating for Urinary Catheter Applications. ACS Biomater. Sci. Eng. *5*, 5825–5832. https://doi.org/10.1021/acsbiomaterials.9b01288.
34. Maheshwari, N., Kottantharayil, A., Kumar, M., and Mukherji, S. (2010). Long term hydrophilic coating on poly(dimethylsiloxane) substrates for microfluidic applications. Appl. Surf. Sci. *257*, 451–457. https://doi.org/10.1016/j.apsusc.2010.07.010.
35. Zhuang, Q., Li, T., Lv, H., Zhang, H., and Zhao, T. (2014). Stable and Homogenous Functionality on PDMS Surface and the Kinetic of Gold Nanoparticle Adsorption on Its Surface. Soft Mater. *12*, 334–338. https://doi.org/10.1080/1539445X.2014.917104.
36. Findenig, G., Kargl, R., Stana-Kleinschek, K., and Ribitsch, V. (2013). Interaction and Structure in Polyelectrolyte/Clay Multilayers: A QCM-D Study. Langmuir *29*, 8544–8553. https://doi.org/10.1021/la400880a.
37. Wu, Y., Zhang, Y., Wang, K., Luo, Z., Xue, Z., Gao, H., Cao, Z., Cheng, J., Liu, C., and Zhang, L. (2021). Construction of Self-Assembled Polyelectrolyte/Cationic Microgel Multilayers and Their Interaction with Anionic Dyes Using Quartz Crystal Microbalance and Atomic Force Microscopy. ACS Omega *6*, 5764–5774. https://doi.org/10.1021/acsomega.0c06181.
38. Mohan, T., Findenig, G., Höllbacher, S., Cerny, C., Ristić, T., Kargl, R., Spirk, S., Maver, U., Stana-Kleinschek, K., and Ribitsch, V. (2014). Interaction and enrichment of protein on cationic polysaccharide surfaces. Colloids Surf. B Biointerfaces *123*, 533–541. https://doi.org/10.1016/j.colsurfb.2014.09.053.
39. Ristić, T., Mohan, T., Kargl, R., Hribernik, S., Doliška, A., Stana-Kleinschek, K., and Fras, L. (2014). A study on the interaction of cationized chitosan with cellulose surfaces. Cellulose *21*, 2315–2325. https://doi.org/10.1007/s10570-014-0267-6.
40. Benselfelt, T., Cranston, E.D., Ondaral, S., Johansson, E., Brumer, H., Rutland, M.W., and Wågberg, L. (2016). Adsorption of Xyloglucan onto Cellulose Surfaces of Different Morphologies: An Entropy-Driven Process. Biomacromolecules *17*, 2801–2811. https://doi.org/10.1021/acs.biomac.6b00561.
41. Rees, D.A. (1969). Conformational analysis of polysaccharides. Part II. Alternating copolymers of the agar–carrageenan–chondroitin type by model building in the computer with calculation of helical parameters. J. Chem. Soc. B *1*, 217–226. https://doi.org/10.1039/J29690000217.
42. Pegueroles, M., Tonda-Turo, C., Planell, J.A., Gil, F.-J., and Aparicio, C. (2012). Adsorption of Fibronectin, Fibrinogen, and Albumin on TiO2: Time-Resolved Kinetics, Structural Changes, and Competition Study. Biointerphases *7*, 48. https://doi.org/10.1007/s13758-012-0048-4.
43. Saftics, A., Prósz, G.A., Türk, B., Peter, B., Kurunczi, S., and Horvath, R. (2018). In situ viscoelastic properties and chain conformations of heavily hydrated carboxymethyl dextran layers: a comparative study using OWLS and QCM-I chips coated with waveguide material. Sci. Rep. *8*, 11840. https://doi.org/10.1038/s41598-018-30201-6.
44. Hussain, M., Wendel, H.P., Schmidt, K., Langer, E., Körber, M.K., Faul, O., Northoff, H., von Heymann, C., and Gehring, F.K. (2018). QCM-D surpassing clinical standard for the dose administration of new oral anticoagulant in the patient of coagulation disorders. Biosens. Bioelectron. *104*, 15–20. https://doi.org/10.1016/j.bios.2017.12.043.
45. Andersson, M., Andersson, J., Sellborn, A., Berglin, M., Nilsson, B., and Elwing, H. (2005). Quartz crystal microbalance-with dissipation monitoring (QCM-D) for real time measurements of blood coagulation density and immune complement activation on artificial surfaces. Biosens. Bioelectron. *21*, 79–86. https://doi.org/10.1016/j.bios.2004.09.026.
46. Chu, A.J., Beydoun, S., Mathews, S.T., and Hoang, J. (2003). Novel anticoagulant polyethylenimine: Inhibition of thrombin-catalyzed fibrin formation. Arch. Biochem. Biophys. *415*, 101–108. https://doi.org/10.1016/S0003-9861(03)00216-9.
47. Dace, R., McBride, E., Brooks, K., Gander, J., Buszko, M., and Doctor, V.M. (1997). Comparison of the anticoagulant action of sulfated and phosphorylated polysaccharides. Thromb. Res. *87*, 113–121. https://doi.org/10.1016/S0049-3848(97)00110-2.
48. Liang, W., Mao, X., Peng, X., and Tang, S. (2014). Effects of sulfate group in red seaweed polysaccharides on anticoagulant activity and cytotoxicity. Carbohydr. Polym. *101*, 776–785. https://doi.org/10.1016/j.carbpol.2013.10.010.
49. Chikha, S.B., Bougatef, H., Capitani, F., Ben Amor, I., Maccari, F., Gargouri, J., Sila, A., Volpi, N., and Bougatef, A. (2023). Composition and Anticoagulant Potential of Chondroitin Sulfate and Dermatan Sulfate from Inedible Parts of Garfish (*Belone belone*). Foods *12*, 3887.
50. Murakami, D., Kobayashi, S., and Tanaka, M. (2016). Interfacial Structures and Fibrinogen Adsorption at Blood-Compatible Polymer/Water Interfaces. ACS Biomater. Sci. Eng. *2*, 2122–2126. https://doi.org/10.1021/acsbiomaterials.6b00415.
51. Kattula, S., Byrnes, J.R., and Wolberg, A.S. (2017). Fibrinogen and Fibrin in Hemostasis and Thrombosis. Arterioscler. Thromb. Vasc. Biol. *37*, e13–e21. https://doi.org/10.1161/ATVBAHA.117.308564.
52. Rabe, M., Verdes, D., and Seeger, S. (2011). Understanding protein adsorption phenomena at solid surfaces. Adv. Colloid Interface Sci. *162*, 87–106. https://doi.org/10.1016/j.cis.2010.12.007.
53. Kargl, R., Bračič, M., Resnik, M., Mozetič, M., Bauer, W., Stana Kleinschek, K., and Mohan, T. (2019). Affinity of Serum Albumin and Fibrinogen to Cellulose, Its Hydrophobic Derivatives and Blends. Front. Chem. *7*, 581. https://doi.org/10.3389/fchem.2019.00581.
54. Wertz, C.F., and Santore, M.M. (2002). Fibrinogen Adsorption on Hydrophilic and Hydrophobic Surfaces: Geometrical and Energetic Aspects of Interfacial Relaxations. Langmuir *18*, 706–715. https://doi.org/10.1021/la011075z.
55. Bagnall, R.D. (1978). Adsorption of plasma proteins on hydrophobic surfaces. II. Fibrinogen and fibrinogen-containing protein mixtures. J. Biomed. Mater. Res. *12*, 203–217. https://doi.org/10.1002/jbm.820120206.
56. Ajdnik, U., Luxbacher, T., and Fras Zemljič, L. (2023). Proteins at polysaccharide-based biointerfaces: A comparative study of QCM-D and electrokinetic measurements. Colloids Surf. B Biointerfaces *221*, 113011. https://doi.org/10.1016/j.colsurfb.2022.113011.
57. Chen, S., Li, L., Zhao, C., and Zheng, J. (2010). Surface hydration: Principles and applications toward low-fouling/nonfouling biomaterials. Polymer *51*, 5283–5293. https://doi.org/10.1016/j.polymer.2010.08.022.
58. Mohan, T., Spirk, S., Kargl, R., Doliška, A., Vesel, A., Salzmann, I., Resel, R., Ribitsch, V., and Stana-Kleinschek, K. (2012). Exploring the rearrangement of amorphous cellulose

model thin films upon heat treatment. Soft Matter *8*, 9807–9815. https://doi.org/10.1039/C2SM25911G.

59. Gericke, M., Liebert, T., and Heinze, T. (2009). Interaction of Ionic Liquids with Polysaccharides, 8 – Synthesis of Cellulose Sulfates Suitable for Polyelectrolyte Complex Formation. Macromol. Biosci. *9*, 343–353. https://doi.org/10.1002/mabi.200800329.
60. Zemljič, L.F., Čakara, D., Michaelis, N., Heinze, T., and Stana Kleinschek, K. (2011). Protonation behavior of 6-deoxy-6-(2-aminoethyl)amino cellulose: a potentiometric titration study. Cellulose *18*, 33–43. https://doi.org/10.1007/s10570-010-9467-x.
61. Dobaj Štiglic, A., Kargl, R., Beaumont, M., Strauss, C., Makuc, D., Egger, D., Plavec, J., Rojas, O.J., Stana Kleinschek, K., and Mohan, T. (2021). Influence of Charge and Heat on the Mechanical Properties of Scaffolds from Ionic Complexation of Chitosan and Carboxymethyl Cellulose. ACS Biomater. Sci. Eng. *7*, 3618–3632. https://doi.org/10.1021/acsbiomaterials.1c00534.
62. Kittle, J.D., Du, X., Jiang, F., Qian, C., Heinze, T., Roman, M., and Esker, A.R. (2011). Equilibrium Water Contents of Cellulose Films Determined via Solvent Exchange and Quartz Crystal Microbalance with Dissipation Monitoring. Biomacromolecules *12*, 2881–2887.
63. Kontturi, K.S., Kontturi, E., and Laine, J. (2013). Specific water uptake of thin films from nanofibrillar cellulose. J. Mater. Chem. A Mater. *1*, 13655–13663. https://doi.org/10.1039/C3TA12998E.
64. Czabany, I., Hribernik, S., Bračič, M., Kurečič, M., Thomas, S., Stana Kleinschek, K., and Mohan, T. (2020). Design of stable and new polysaccharide nanoparticles composite and their interaction with solid cellulose surfaces. Nano-Structures & Nano-Objects *24*, 100564. https://doi.org/10.1016/j.nanoso.2020.100564.
65. Jachimska, B., Świątek, S., Loch, J.I., Lewiński, K., and Luxbacher, T. (2018). Adsorption effectiveness of β-lactoglobulin onto gold surface determined by quartz crystal microbalance. Bioelectrochemistry *121*, 95–104. https://doi.org/10.1016/j.bioelechem.2018.01.010.

STAR★METHODS

KEY RESOURCES TABLE

REAGENT or RESOURCE	SOURCE	IDENTIFIER
Chemicals, peptides, and recombinant proteins		
Fucoidan (Fu: ≥95%) from Fucus vesiculosus	Fluka Chemie GmbH (Germany)	CAS: 47865
Chondroitin sulfate (CS Average MW 20,000 - 30,000)	Carbosynth (Staad, Switzerland)	CAS: YC31416
kappa-Carrageenan from red algae (20, 000 – 30, 000)	Carbosynth (Staad, Switzerland)	CAS: YC30039
ε-polycaprolactone (P; average molecular weight: 80 kDa)	Sigma Aldrich, Germany	CAS: 440744
polyethyleneimine (PE, branched average Mw ~25 kDa	Sigma, Aldrich Germny	CAS: 408727
Heparin sodium salt	Carbosynth (Staad, Switzerland)	CAS: 9041-08-1
Cellulose sulfate	Self produced	Self produced
Gold coated quartz crystals	Biolin Scientific	CAS: QSX301
Citrated normal human blood plasma	Stago, Austria	CAS:00982
Pathromtin SL	Stago, Austria	CAS: 00595
0.025 M $CaCl_2$ solution	Stago, Austria	CAS:00367
Experimental models: cell lines		
Primary human pulmonary artery endothelial cells (hECs)	Lonza (Allendale, New Jersey)	CAS: 2530
Other		
Gold coated quartz crystals	Biolin Scientific	CAS: QSX301
Two-burette automatic titrator T70	Mettler Toledo (Switzerland)	https://www.mt.com/us/en/home/phased_out_products/Laboratory_Analytics_Browse/Product_Family_Browse_titrators_main/Titration_excellence_family_main/T70_Titrator_1.html
Automatic titration unit DL 53	Mettler Toledo (Switzerland)	https://www.mt.com/us/en/home/phased_out_products/PhaseOut_Ana/DL53.html
Thrombotrack™ Solo coagulometer	Axis-Shield PoC (Scotland).	http://www.medista.cz/data/files/technoclone_thrombotrack_solo_brochure.pdf
QCM-D instrument (model E4)	Biolin scientific (Götenburg, Sweden)	https://www.biolinscientific.com/qsense/instruments/qsense-analyzer
UV/Vis spectrophotometer Cary 60	Agilent Technologies (Santa Clara, USA)	https://www.agilent.com/en/product/molecular-spectroscopy/uv-vis-uv-vis-nir-spectroscopy/uv-vis-uv-vis-nir-systems/cary-60-uv-vis-spectrophotometer
Zeiss LSM510 META confocal imaging system with planeofluar X40/1.3 oil DIC objective	Carl Zeiss GmbH (Jena Germany).	https://www.bio.umass.edu/microscopy/Guided_Tour_for_LSM_510_and_META.pdf
Agilent 7500 AFM multimode scanning probe microscope	Keysight Technologies (Santa Barbara, USA).	https://www.keysight.com/us/en/assets/7018-04194/data-sheets/5991-3639.pdf
DEKTAK 150 Stylus Profiler	Veeco (Plainview, NY, U.S.A.).	http://www.eicsac.com/dektak150.pdf
TFA XPS instrument	Physical Electronics GmbH (Feldkirchen/Münich, Germany)	https://www.phi-gmbh.eu/

(*Continued on next page*)

Continued

REAGENT or RESOURCE	SOURCE	IDENTIFIER
OCA35 contact angle measurement system	Dataphysics (Germany)	https://www.dataphysics-instruments.com/products/oca/
SurPASS 3	Anton Paar GmbH, (Graz,Austria)	https://www.anton-paar.com/si-en/products/details/surpass-3/

RESOURCE AVAILABILITY

Lead contact

Further information and requests for resources and reagents should be directed to and will be fulfilled by the lead contact, Tamilselvan Mohan (tamilselvan.mohan@tugraz.at).

Materials availability

All data supporting the newly fabricated inks and 3D scaffolds can be found within the manuscript and the supplemental information or can be received from the lead contact upon request.

This study did not generate new unique reagents.

Data and code availability

- Data: All data reported in this paper will be shared by the lead contact upon request.
- Code: This paper does not report original code.
- Any additional information required to reanalyze the data reported in this paper is available from the lead contact upon request.

EXPERIMENTAL MODEL AND STUDY PARTICIPANT DETAILS

Cell lines

Human Pulmonary Artery Endothelial cells (cat# CC-2530) purchased from Lonza were grown in EGM-2 media (cat# CC-4176; Lonza) supplemented with EGM2 Bulletkit and 10% fetal bovine serum (FBS). Cells were cultured at 37°C with 5% CO_2 and used from passages 4–7.

METHOD DETAILS

General material details

Fucoidan (Fu: ≥95%) from Fucus vesiculosus, κ-Carrageenan (Carr), chondroitin sulfate (CS sodium salt from shark cartilage, ε-polycaprolactone (P; average molecular weight: 80 kDa), polyethyleneimine (PE, branched average Mw ~25 kDa), chloroform (≥99%), phosphate buffered saline (PBS) tablet, sodium chloride (NaCl, ACS reagent, ≥99.0%) and cover glasses (22 mm × 22 mm) were purchased from Sigma-Aldrich, Austria. Heparin sodium salt (Hep) from porcine intestinal mucosa was purchased from Carbosynth (Staad, Switzerland). Cellulose sulfate (CellS) was synthesized following the published literature (see below for a bief description).[59] Gold coated quartz crystals (Au-sensors, QSX301) were purchased at Biolin scientific, Sweden. 4-well chamber glass slides for cell culturing experiments were purchased from ibidi@cell in focus, Austria. Citrated normal human blood plasma, pathromtin SL and 0.025 M $CaCl_2$ solution were purchased at Hypen Biomed, France. Ultra-pure water with a resistivity >18 MΩ cm (Millipore, USA) was used for the preparation of all aqueous systems in this work.

Cellulose sufate synthesis

To a solution of 45.0 g of BMIMCl, 5.0 g (30.8×10^{-3} mol) of spruce sulfite pulp (SSP), and 70 mL of DMF, 6.87 g (43.2×10^{-3} mol) of SO3/pyridine were added under vigorous stirring. After 2 h at 25°C, 70 mL of 1 M NaOH and 160 mL of water were added. The clear solution, formed after about 5 min stirring, was precipitated into 1 L of isopropyl alcohol/water (9:1). To remove residual imidazolium cations attached to the negatively charged polymer, the product was dissolved twice in 300 mL of a 2% NaCl solution and twice in 300 mL of water, and each time precipitated into 1 L of isopropyl alcohol/water (9:1). The obtained polymer was washed with 150 mL of isopropyl alcohol/water (8:2) and finally purified by freeze-drying.

pH-potentiometric titration

The charge density of carboxylic groups of all sulfated polysaccharides was determined by acid-base titration using a two-burette automatic titrator T70 (Mettler Toledo, Switzerland). The burettes were filled with 0.1 mol L^{-1} HCl and 0.1 mol L^{-1} KOH as titrants. The analyte was prepared by dissolving 0.1 g of sulfated polysaccharide in ultra-pure water and adjusting the ionic strength to 0.1 mol L^{-1} by addition of 3 mol L^{-1} KCl solution. The analyte was titrated in a forward (acidic to alkaline) and backward (alkaline to acidic) manner between $2 < pH < 10$ in an inert atmosphere (N_2 gas purging). The pH value was recorded using a combined glass electrode DG111-SC (Mettler Toledo, Switzerland). All

measurements were repeated thrice. A blank HCl–KOH titration was carried out under the same conditions as the analyte. The charged density of carboxylic groups was determined by plotting Q/m (pH) titration isotherms. Where Q/m represents the charge density of functional groups per mass of sample in mmol/g. The total charge was obtained as follows. The ionic species present in the titration system are H^+, OH^-, their counter ions K^+ and Cl^- as well as the species of interest, denoted as A_k^n, where n is the charge number and k is the enumerator. The total charge Q, due to the presence of A_k^n is calculated using the electro-neutrality condition according to Equation 1:

$$Q(pH) = FV_t \sum_k n[A_k^n] = FV_t([Cl^-] - [K^+] + [OH^-] - [H^+]) \quad \text{(Equation 1)}$$

where square brackets denote the ion concentrations in mol/dm^3, V_t the total volume and F the Faraday's constant. The potassium and chloride ion concentrations, $[K^+]$ and $[Cl^-]$, respectively, are known from the titrant additions, while the hydrogen and hydroxyl ion concentrations, $[H^+]$ and $[OH^-]$, respectively, are measured with a pH meter. In a blank titration without the species of interest only H^+, OH^-, K^+, and Cl^- ions are present, thus $Q = 0$ for any given pH. This allows replacing the $[OH^-]$–$[H^+]$ term in Equation 1 by the difference $[K^+]_{blank}$–$[Cl^-]_{blank}$ and results in (Equation 2):

$$Q_{AC}(pH) = FV_t([Cl^-] - [K^+] + [K^+]_{blank} - [Cl^-]_{blank}) \quad \text{(Equation 2)}$$

The latter approach is recommended because it permits eliminating the error due to the presence of dissolved carbon dioxide in the titration system.[60,61]

Polyelectrolyte titration

The charge density of sulfphate groups of all polysaccharides was determined by titration with an oppositely charged polyelectrolyte using an automatic titration unit DL 53 (Mettler Toledo, Switzerland). The cationic polyelectrolyte polydiallyldimethyl ammonium chloride (pDADMAC; c = 1 mmol L^{-1}) was used as a titrant. The analyte was prepared by adding 0.5 mL of an aqueous polysaccharide solution (c = 0.2 wt.%) and 0.5 mL of Toluidine blue indicator (c = 0.1 mmol L^{-1}) to 40 mL of ultra-pure water. The analyte was titrated by incremental titrant additions until the equivalent point was reached. The equivalent point was determined spectroscopically at a wavelength of 660 nm using a DP 5 phototrode (Mettler Toledo, Switzerland). Each titration was performed three times at neutral pH assuring full ionisation of sulphate groups. Polyelectrolyte titration was used as an alternative to pH-potentiometric titration, since the strongly acidic sulphate esters cannot be protonated in the pH region used in pH-potentiometric titrations and can therefore not be quantified.[19]

Sample preparation

Preparation of polyethyleneimine (PE) solution: PE (0.1 wt.%) was dissolved in Milli-Q-water. The ionic strength of the solution was adjusted to 150 mM with sodium chloride (NaCl) at pH 7.4.

Preparation of sulfated polysaccharide solution

The sulfated polysaccharides were dissolved at a concentration of 0.2 wt.% in MilliQ-water and the ionic strength of the solution was adjusted to 150 mM NaCl. The pH of the solution was adjusted to 7.4 by using either 0.1 M NaOH or 0.1 M HCl. Afterwards, the solutions were filtered using 0.2 μm PTFE filter.

Preparation of fibrinogen (Fib) solution

Fib (3 mg mL^{-1}) was dissolved in PBS buffer prepared by dissolving one tablet per 200 mL of water (yielding 10 mM phosphate buffer, 2.7 mM potassium chloride, and 137 mM sodium chloride at pH 7.4) at room temperature.

In-vitro hemocompatibility evaluation

Activated partial thromboplastin time (APTT)

The latter indirectly measures the action of thrombin by detecting the formation of fibrin from fibrinogen.[14] APTT experiment was performed by mixing 80 μL of citrated normal human blood plasma (ORKE41, Dade Behring) with 20 μL of sulphated polysaccharide solutions in 0.9 wt.% NaCl. To this, 100 μL of Pathromtin SL reagent (ORHO37, Dade Behring), acting as a coagulation pathway activator, was added. The concentration of the polysaccharides in the final mixture ranged from 0.5 – 15 mg mL^{-1}. The mixture was incubated at 37°C for 3 minutes followed by addition of 100 μl of 0.025 M $CaCl_2$ solution (equilibrated to 37°C) triggering the coagulation cascade. The coagulation time was determined using a Thrombotrack™ Solo coagulometer (Axis-Shield PoC, Scotland). Normal blood plasma without addition of polysaccharide was measured in the same way as a reference to which all polysaccharide data were normalized. To keep the same solution ratio as in cases where polysaccharides were added, an additional amount of 0.9% NaCl was added. All measurements were repeated thrice.

Preparation of polycaprolactone (P) thin films

Thin films of polycaprolactone (P) were prepared on Au-sensors, round cover glasses (diameter: 1 cm) and on 8-well chamber glass slides for QCM-D, hemocompatibility and for cell culturing experiments. The Au-coated sensors were cleaned prior to film preparation: The sensors

were initially soaked into a mixture of H_2O/H_2O_2 (30 wt.%)/NH_4OH (5:1:1; v/v/v) for 10 min at 70°C. Afterwards, they were immersed in "piranha" solution (H_2O_2 (30 wt.%)/H_2SO_4 (98 wt.%) (1:3; v/v)) for 60 s, rinsed with water, and blow-dried with N_2 gas. The round cover glasses were rinsed with absolute ethanol, rinsed with water and blow dried with N_2 gas. For spin coating on Au-sensors and cover glasses (22 mm × 22 mm), 70 μL of the P solution (1 wt.%, dissolved in chloroform) was used. Whereas 150 μL P solution was used for coating of each chamber of the 8-well chamber glass slides. The films were spin coated at a spinning speed of 4000 rpm, an acceleration of 2500 rpm s^{-1} for 60 s using a Polos MCD wafer spinner (APT corporation, Germany).[17,30] All P substrates were dried with nitrogen gas and stored under ambient conditions until further use.

Quartz crystal microbalance with dissipation (QCM-D)

A QCM-D instrument (model E4) from Q-Sense (Gothenburg, Sweden) was used for the functionalization of P films with sulfated PS, D_2O/H_2O exchange, adsorption of fibrinogen and for the anticoagulant studies. The instrument simultaneously measures changes in the resonance frequency (Δf) and energy dissipation (ΔD) of the oscillating piezoelectric crystal arising from the changes in its mass and elasticity upon adsorption or desorption of components and ions from the aqueous solutions. If the elasticity of the adsorbed coatings insignificantly differs from that of the crystal, the mass of adsorbed coatings can be related to Δf by the Sauerbrey equation as follows:

$$\Delta m = C\frac{\Delta f_n}{n} \quad \text{(Equation 3)}$$

where Δf_n is the observed frequency shift, C is the Sauerbrey constant (− 0.177 mg Hz^{-1} m^{-2} for a 5 MHz crystal), n is the overtone number (n = 1, 3, 5, etc.), and Δm is the change in mass of the crystal.

The dissipation energy (D) refers to the frictional losses that lead to damping of the oscillation depending on the elastic properties of the material. D is defined as:

$$D = \frac{E_{diss}}{2\pi E_{stor}} \quad \text{(Equation 4)}$$

where E_{diss} is the energy dissipated and E_{stor} is the total energy stored in the oscillator during one oscillation cycle.

Functionalization of polycaprolactone (P) thin films with sulphated PS

Briefly, the P coated Au-sensors were mounted into the QCM-D flow cell and the initial resonance frequency of the sensor was determined. Then, the P films were equilibrated with water followed by 150 mM NaCl solution until a stable resonance frequency was established. Afterwards, the PE solution (0.1 wt.%, dissolved in 150 mM NaCl) was pumped through the QCM-D cells for 30 minutes followed by rinsing with 150 mM NaCl solution (pH 7.4) for 10 minutes. Following this step, aqueous solutions of sulfated PS (c = 0.2 wt.%, in 150 mM NaCl) were pumped over the PE layer for 30 min. After this, the PS solution was exchanged with NaCl (10 minutes) and water (30 minutes), respectively. The liquid flow rate and temperature was kept at 0.1 mL min^{-1} and 21 ± 0.1°C throughout the experiments. The coated sensors were taken out from the flow cell, dried by N_2 gas, and stored at room temperature for further use.

For *in-vitro* hemocompatibility evaluation, the sulphated PS coatings were prepared on cover glasses following the QCM-D procedure. In this case, the P films coated cover glasses were transferred to a 24-well plate (well volume of 2 mL) followed by subsequent exchange of solutions: NaCl (10 minutes), PE (30 minutes), NaCl (10 minutes), SPS (30 minutes), NaCl (10 minutes), and MilliQ-water (30 minutes).

For cell culturing experiments, the SPS were coated on 4-well chamber glass slides coated with P films. The coating of PS layers was performed using the same protocol as described for glass cover classes. All coated glass substrates were dried with N_2 gas and stored under ambient conditions until further use.

All measurements were performed in triplicates and arithmetic mean curves are shown as results.

Adsorption of endothelial cell culture medium-2

The stability of the SPS coating was investigated using adsorption with endothelial cell culture medium-2 (EGM-2). SPS-coated crystals were assembled in the QCM flow cells and equilibrated with MilliQ water. After establishing a stable frequency with MilliQ water, the EGM-2 medium was introduced into the flow cell for 24 hours at 37°C (flow rate: 0.1 mL min^{-1}). Following this, the surfaces were rinsed with MilliQ water until a stable change in frequency was observed. This experiment was repeated at least three times for each SPS coating.

D_2O/H_2O exchange studies

Water content of uncoated and coated P films was determined using a water deuterium exchange as described previously.[58,62–64] The coated crystals were placed in the QCM flow cell and equilibrated with MilliQ-water until a stable frequency was obtained (t∼ 60 minutes). Subsequently, the experiments were restarted and a baseline in MilliQ-water was set up for 10 min. After this, MilliQ-water was exchanged with D_2O for 20 minutes. Then, D_2O was exchanged with MilliQ-water for 15 minutes. Afterwards, the experiments ended. The D_2O/H_2O exchange studies for each coating were performed at least four times.

Adsorption of fibrinogen (Fib)

After equilibration of the PS coated films in 150 mM NaCl, water and PBS buffer solution at a pH value of 7.4, the fibrinogen (Fib, 3 mg mL^{-1}, dissolved in 10 mM PBS buffer) was introduced into the QCM flow cell for 30 minutes followed by PBS buffer solution for 30 minutes. The flow rate was kept at 0.1 mL min^{-1} throughout all experiments. The temperature was kept 37 $\pm$ 0.1°C for all experiments. Each adsorption experiment was repeated thrice.

Clotting formation and time determination

The P coated Au-sensors with and without sulphated PS coating were mounted in an open QCM-D cell made of poly(tetrafluoroethylene) for the coagulation experiments. The open cell allows adding of reactants manually through a round opening during measurements. In this fashion, 100 μL of citrated normal human blood plasma (ORKE41, Dade Behrin), equilibrated to 37°C, was deposited on the mounted sensors. After 2 minutes of baseline establishment, the coagulation was triggered by adding 100 μL of aqueous 0.025 M $CaCl_2$ solution (ORKE41, Dade Behring). The experiments were conducted until stable Δf and ΔD were obtained, signalling the end of the coagulation process. All experiments were carried out in triplicates at a constant temperature of 37 $\pm$ 0.1°C, and their arithmetic mean curves are shown as results. The Δf and ΔD as a function of time give details about the onset thrombin formation time, fibrin deposition rate (df/dt), and total coagulation time.

Whole blood adhesion

The whole blood adhesion test was performed to evaluate the blood compatibility of the polysaccharide-coated P films. For this purpose, polysaccharide-coated P films were prepared on casted P films (10 × 50 mm) and immersed into individual polystyrene cuvettes containing 3 mL of whole blood (with 10 wt.% sodium citrate anticoagulants, collected from healthy individual at the university clinical center, UKC Maribor) at 37°C. For the instant test, the P film was taken out from the whole blood after 5 minutes and immersed in individual cuvettes filled with MilliQ- water (3 mL) to release the haemoglobin of adhered red blood cells on the surface. After shaking at 37°C for 1 h, the solution from the cuvettes was transferred into a fresh cuvette and its absorbance (abs) at 415 nm was recorded with UV/Vis spectrophotometer. For the long-time test, the P films were immersed taken out from the whole blood after 60 min. The experiment was repeated at least four times.

Cell culture

Before the cell culturing experiments, the uncoated and coated P cover slides were exposed to UV-light for 15 minutes followed by rinsing with PBS buffer and blown dry with N_2 gas. Primary human pulmonary artery endothelial cells (hECs) were obtained from Lonza (Allendale, New Jersey) and were cultured according to the manufacturer's instructions. Endothelial specific media with growth factor supplements (EBM-2, Lonza) was used and changed every third day.

Cell adhesion and viablity

For cell adhesion assays, cells were suspended in EGM-2 culture medium at a density of 0.75 × 10^5 cells/mL. A volume of 200 μL (20,000 cells) was seeded on each surface and left to adhere for 6 h. Afterwards, the surfaces were washed with PBS (1×) to remove non adherent cells. Remaining adhered cells were stained with F-actin, the cells on the respective coated cover slide and washed with PBS and fixed with 4% formaldehyde for 30 min at 4°C. Then the cells were incubated with Alexa555 conjugated-phalloidin (Molecular Probes) for 20 minutes at room temperature followed by repetitive washing with PBS and mounting with anti-fading embedding medium (Vector Laboratories) containing DAPI counterstaining to visualize the nucleus. Immunostained slides were scanned with an Aperio slide scanner-microscope and images were captured with Image Scope software (Aperio, Oxford, UK). The Cell nuclei stained with DAPI were expressed as number of adherent cells cm^{-2}.

The cell viability of the primary hECs was assessed using a cell counting kit 8 (CCK8) according to the manufacturer's instructions (Dojindo Molecular Technologies, Inc). Briefly cells (20,000 cells/well) were incubated in 4-well glass chamber plates for 24 h on different coatings. Subsequently, 10 μl CCK-8 per 100 μl culture medium was added to each well, and the cells were incubated for 3 h at 37°C. Later the supernatants were transferred to a 96 well plate, where cell viability was assessed as absorbance of each well at 450 nm measured by a microplate reader. The absorbance values were normalized to the total protein concentration of the correspondent surface treated cells. All the experiments were performed in triplicates.

Description of cellular morphology

Four morphologic parameters: area and perimeter, were measured and averaged for at least 50 cells for each type of coatings. These morphologic parameters were expressed as percentage of the respective parameter value for the control condition. P coatings were used as the control (scale bar 100 μm). Numerical values are given as mean $\pm$ SEM.

Surface analytics

Atomic force microscopy (AFM)

The surface morphology of the samples was characterized by AFM in tapping mode with an Agilent 7500 AFM multimode scanning probe microscope (Keysight Technologies, Santa Barbara, USA). The samples were scanned using silicon cantilevers (ATEC-NC-20, Nanosensors,

Germany) with a resonance frequency of 210–490 kHz and a force constant of 12–110 Nm^{-1}. All measurements were performed at ambient temperature. All images were recorded with a resolution of 2048 × 2048 pixels and were processed using the freeware Gwyddion allowing for the AFM roughness to be calculated as the root-mean-square (rms) deviation from the mean height of the topography after levelling of the images by mean plane subtraction.

Profilometry

Layer thickness of the uncoated and coated P coated films was determined by profilometry using a DEKTAK 150 Stylus Profiler from Veeco (Plainview, NY, U.S.A.). The scan length was set to 1000 μm over the time duration of 3 s. The diamond stylus had a radius of 12.5 μm and the force was 3 mg with a resolution of 0.333 μm/sample and a measurement range of 6.5 μm. The profile was set to hills and valleys. Prior to the surface scanning, the coating was scratched to remove the PCL films in order to determine the thickness of the coating using a step-height profile. The thickness was determined at 3 independent positions.

X-Ray photoelectron microscopy (XPS)

XPS spectra were recorded with a Thermo Scientific K-Alpha X-ray Photoelectron Spectrometer (XPS) equipped with an Al X-ray source (1486.6 eV) operating with a base pressure in the range of 10^{-8}-10^{-10} mbar. Survey scans were acquired with a pass energy of 100 eV and a step size of 1.0 eV. All spectra were normalized to the Au 4f7/2 peak. The average chemical composition was calculated from wide scan spectra obtained at two different locations on each surface. All analyses were performed at ambient temperature.

Wettability

Static water contact angle measurements (SWCA) were conducted by using an OCA15+ contact angle measurement system (Dataphysics, Germany) to quantify the wettability of sulphated polysaccharide coatings. SWCA measurements were conducted at room temperature using ultra-pure water on at least two independent surfaces with a drop volume of 3 μL. Each SWCA value was the average of at least five drops of liquid per surface.

Streaming potential measurements

The surface ζ-potential was determined from the measurement of streaming current using the instrument SurPASS 3 (Anton Paar GmbH, Austria) and an Adjustable Gap Cell for 14 mm discs. The streaming current measurement was used as an alternative to streaming potential measurement because of the additional conductivity caused by the Au QCM-D sensor.[65] A pair of QCM-D sensors with the same upper coating was fixed on the sample holders (with a circular cross-section and a diameter of 14 mm), using double-sided adhesive tape with weak adhesion to ease the removal of the QCM-D sensors after completing the measurement series. The distance between adjacent sensor discs was adjusted to 103 ± 4 μm during several rinsing step cycles with the 10 mM KCl aqueous solution. The streaming current was measured with an Ag/AgCl electrode. The ζ-potential as a function of pH was determined in an aqueous solution of 10 mM NaCl (the ionic strength was high enough to suppress any contribution of interfacial conductivity according to Jachimska et al.[65] During the pH scan measurement, the pH was adjusted with 0.05 M HCl and 0.05 M NaOH. By means of surface ζ-potential analyses, the aqueous electrolyte solution was purged with nitrogen gas.

QUANTIFICATION AND STATISTICAL ANALYSIS

Statistical analysis was performed using Prism 5 (GraphPad, San Diego, CA, USA). The student's t-test was used for nonparametric data. P-values <0.05, 0.01, 0.001 were considered statistically significant.